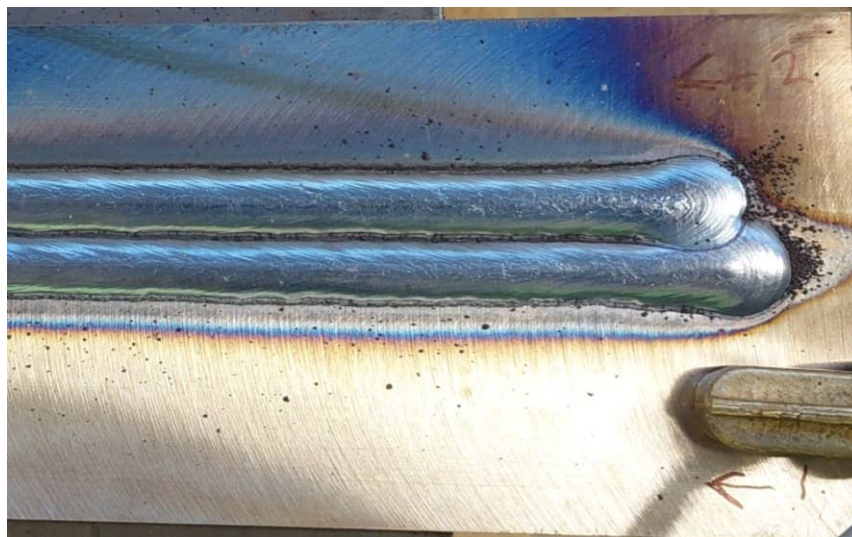


## RESEARCH REPORT

VTT-R-00140-24  
Replaces research report VTT-R-00642-23



# MICWEST - Influence of environment and microbes on corrosion behaviour of welded steels in the LILW repositories: annual report 2023

Authors: Amina Alimbekova, Thomas Ohligschläger, Maija Nuppenen-Puputti, Quynh Nguyen, Pekka Nevasmaa, Vilma Ratia-Hanby

Confidentiality: VTT Public

Version: 23.2.2024



<b>Report's title</b> MICWEST - Influence of environment and microbes on corrosion behaviour of welded steels in the LILW repositories: annual report 2023	
<b>Customer, contact person, address</b> SAFER2028 (National Nuclear Safety and Waste Management Research Programme 2023-2028)	<b>Order reference</b>
<b>Project name</b> Influence of environment and microbes on corrosion behaviour of welded steels in the LILW repositories	<b>Project number/Short name</b> 135883 / MICWEST
<b>Author(s)</b> Amina Alimbekova, Thomas Ohlgschläger, Maija Nuppenen-Puputti, Quynh Nguyen, Pekka Nevasmaa, Vilma Ratia-Hanby	<b>Pages</b> 39/13
<b>Keywords</b> Corrosion, LILW repository, steel, weld, MIC, water chemistry	<b>Report identification code</b> VTT-R-00140-24
<p><b>Summary</b></p> <p>This is the first research report of the MICWEST project, included in the SAFER2028 programme. The objective of MICWEST is to study the performance of steel welds in low- and intermediate level waste (LILW) repository mimicking conditions. This will be done through defining the type of corrosion in welds and heat-affected zones (HAZ) in different conditions mimicking the different evolutionary stages of the repository, studying microbe-weldment interactions on steel surfaces and defining the role of different weldment types, material combinations in welds and post-weld cleaning methods on weld durability and corrosion resistance. The current report illuminates the background knowledge of the conditions assumed to prevail in the repositories, and describes the selection of certain water types, materials and welding methods to be assessed within the project.</p> <p>It is assumed that the repository will undergo evolution in its conditions and thus the conditions will change over time. This research will consider cases in which water will get into contact with the steel material and welds. In the first stages of the repository, porewater from the concrete present in the repository is going to have a major effect on the constituents of the water. Due to the ingress of the groundwater, the porewater will get mixed with the groundwater, and its influence will lessen until the water can be considered to be fully groundwater. In this report, thermodynamical simulations on the water chemistry are presented in order to improve the understanding of the principles of the interaction of groundwater with cured cement that contains concrete porewater. Moreover, baseline electrochemical assessment for the selected stainless steels is included for simulated porewater and groundwater at different pH.</p> <p>Native groundwaters were collected and analysed, and recipes for simulants were formulated. The activity of the intrinsic groundwater microbes will be assessed for the next phase of the project, consisting of exposure tests.</p> <p>The materials and the welding methods were selected to represent the components present in the repository:</p> <ol style="list-style-type: none"> <li>(1) Carbon steel containers to include the cut-up waste: carbon steel welded by submerged arc welding due to its high productivity and quality in workshop conditions, and MAG welding for its versatility in all-position butt and fillet welds in workshop and field on-site fabrication.</li> <li>(2) Weld between the reactor pressure vessel nozzle and plug to shut the reactor pressure vessel: the inside of the reactor pressure vessel clad with 321 stainless steel is welded with the plug material of stainless steel 316L with MAG welding, due to its versatility in all-position welds also in on-site fabrication.</li> <li>(3) Weld between the outside of the reactor pressure vessel nozzle and plug, and reactor pressure vessel and new lid: reactor pressure vessel steel is welded with stainless steel 316L (plug/lid) with MAG welding due to its versatility in all-position welds also in on-site fabrication.</li> </ol> <p>These welds were manufactured to provide testing materials for the next phases, consisting of exposure tests. In addition, a part of the samples will be post-treated by either grinding or pickling.</p>	
<b>Confidentiality</b>	VTT Public
23.2.2024	
<b>Written by</b> Vilma Ratia-Hanby, Research Scientist	<b>Reviewed by</b> Andressa Trentin, Research Scientist
<b>VTT's contact address</b> VTT Technical Research Centre of Finland Ltd., P.O. Box 1000, FI-02044 VTT, Finland	
<b>Distribution (customer and VTT)</b> SAFER2028, VTT Register office	
<i>The use of the name of "VTT" in advertising or publishing of a part of this report is only permissible with written authorisation from VTT Technical Research Centre of Finland Ltd.</i>	



## Approval

### VTT TECHNICAL RESEARCH CENTRE OF FINLAND LTD

Date:

26 February 2024

Signature:

DocuSigned by:  
*Janne Pakarinen*  
C91D5DDA5EC5446...

Name:

Janne Pakarinen

Title:

Research Team Leader



## 1. Preface

---

The MICWEST project, in which this report has been written, is a part of the SAFER2028 (National Nuclear Safety and Waste Management Research Programme 2023-2028). In this first report of the project, the background of the project and its materials are presented. Vilma Ratia-Hanby has worked as the project manager, and Amina Alimbekova, Maija Nuppenen-Puputti, Thomas Ohlgschläger, Pekka Nevasmaa and Quynh Nguyen (all in BA5507) have been participating in the work. In addition, personnel from BA5507 (Taru Lehtikuusi, Jukka Maunumäki, Hanna Iitti, Tuomo Kinnunen and Arto Nyholm) and BA5203 (Mirva Pyrhönen and Malin Bomberg) have participated in the work. Special thanks are given to Seppo Peltonen (BA4509) for the welding. The work has been funded by National Nuclear Waste Management Fund (VYR) and VTT. Fortum Oyj and TVO have facilitated the fetching of the natural groundwaters, which is gratefully acknowledged. Sophie Ehrnrooth is thanked for her help in organising the welding at Taitotalo, Helsinki.



## Contents

---

1.	Introduction.....	5
1.1	Goal and limitations .....	5
2.	Background .....	5
2.1	Low and intermediate level waste .....	6
2.2	Disposal of low and intermediate level radioactive waste in repositories.....	6
2.2.1	Systems involved / containers and whole reactors to be put into the repository .....	7
2.2.2	Surrounding environment and its influence on the durability of the LILW containers and the safety of LILW repositories.....	7
2.2.3	Materials involved.....	8
2.3	Waters.....	8
2.3.1	Assumed phases of the repositories .....	8
2.3.2	Pore water .....	9
2.3.3	Groundwaters (+ Differences in sites).....	9
2.4	Corrosion and its affecting factors .....	11
2.4.1	MIC-related occurrences and previous findings .....	13
2.4.2	Microbiology related to the LILW repositories .....	14
3.	Materials and methods .....	15
3.1	Materials.....	15
3.1.1	Steels .....	15
3.1.2	Welded steels.....	16
3.1.3	Waters .....	16
3.2	Methods .....	17
3.2.1	Welding .....	17
3.2.2	Electrochemical methods.....	18
3.2.3	Optical microscopy .....	18
3.2.4	Microbiological methods .....	19
3.2.5	Water chemistry.....	21
4.	Results .....	21
4.1	Electrochemical measurements.....	21
4.2	Surface analysis .....	23
4.3	Water chemistry simulations .....	24
4.3.1	Simulation excluding the formation of magnesium and calcium silicates.....	27
4.3.2	Simulation including the formation of magnesium and calcium silicates.....	29
4.3.3	Validity of the thermodynamic simulation results.....	31
4.4	Enumeration of microbial cell counts in repository site waters .....	33
4.5	Water chemistry of the repository site groundwaters .....	33
5.	Summary .....	35
6.	References .....	36
7.	Appendix .....	



## 1. Introduction

---

The establishment of low and intermediate level waste repositories represents a critical component of Finland's comprehensive approach to nuclear waste management. A low and intermediate level waste (LILW) repository is a specialized facility designed to safely dispose of radioactive waste generated from various sources, such as nuclear power plants, research institutions, and medical facilities. These repositories employ multiple engineered barriers, including containment structures comprising of layers of steel and concrete, to isolate the waste from the environment and minimize the risk of radiation exposure to both humans and the ecosystem. The waste is typically packaged in accordance with strict regulations, and its disposal follows rigorous safety protocols to ensure long-term stability and safety. Such repositories play a crucial role in the responsible and sustainable management of radioactive waste, safeguarding public health and the environment for generations to come.

MICWEST will study the corrosion behaviour of steel welds simulating conditions in Finnish LILW repositories, considering the environment at the planned disposal sites throughout their evolution: the ingress of groundwater, the ageing of concrete which is used as a release barrier, and the microbiological activity. The response of the weld joints to the corrosive environment is important, because their corrosion behaviour often differs from the bulk material. The factors that are affecting the corrosion resistance are defined by testing within the project welded joints manufactured with different methods and post-processing in various conditions simulating water in LILW repositories, including microbial content and different chemistries.

The results described in the following report mostly concern the preparation, processing, modelling, and baseline establishment for the main part of the work. The corrosion mechanisms of bulk stainless steels 316L and 321 are studied to establish a comparison baseline to the welds. Welds are prepared for the electrochemical, short- and long- term tests. Native waters from the example repository sites are tested, and their microbial content is outlined. Also, modelling of the concrete-water interactions is performed to consider the possible buffers and final pH values in the repository conditions. As methods, electrochemical tests are used to measure corrosion rates, microscopy to identify corrosion, as well as microbiological methods to define the microbial content of the native groundwaters.

### 1.1 Goal and limitations

The MICWEST project studies the performance of steel weldments in LILW repository mimicking conditions. Its main objectives are to produce new knowledge on the behaviour and durability of weldments and welded joints of steels during the evolution of the LILW repositories, to define microbe-weldment interactions on steel surfaces and to reveal weld-attached microbial community structures, and to define the role of different weldment types, material combinations in welds and post treatment methods on weld durability and corrosion resistance. The goal of this report is to document the background and process of selecting the waters, materials and welding methods used in the project. It includes baseline measurements of the corrosion behaviour of the stainless steels 316L and 321. The results of the welds are not included; they will be presented in the following reports and publications.

## 2. Background

---

This chapter consists of describing the background on the low and intermediate level waste repositories and the waters present in the bedrock surrounding the repositories.

## 2.1 Low and intermediate level waste

Nuclear waste according to the Nuclear Energy Act (Ydinenergi laki (990/1987) is defined as a spent fuel or materials and structures that have become radioactive and were removed from their use from nuclear power plant operations. The act also specifies that the nuclear waste produced from the nuclear energy use in Finland needs to be handled, stored, and permanently disposed of in Finland. Depending on the nature and activity concentration of the waste, The Radiation and Nuclear Safety Authority (STUK) defines such waste in Regulation STUK Y/4/2018 (Radiation and Nuclear Safety Authority, 2018).

The solid and liquid waste derived from the operation of nuclear power plants (NPP) can be categorised as (IAEA, 2009): very low-level waste (VLLW), low level waste (LLW), intermediate level waste (ILW). It is hard to sharply categorize the waste as the limits of the activity concentration can differ according to the groups of radionuclides. So, depending on the disposal facility design and disposal planning the low and intermediate waste can be coupled into the low and Intermediate level waste (LILW) (IAEA, 1998).

A large portion of LILW comes from the objects and materials related to the treatment of radioactive liquids, resins, filter materials, evaporator residues, etc. Also, low level waste may include activated reactor hardware, discarded equipment, tools, or contaminated trash from daily operations. Typical items may include no longer usable clothing of the personnel, papers and other items for cleaning, miscellaneous contaminated parts from the maintenance, wood, dirt, glass, and other scraps (Äikäs & Anttila, 2008).

The mentioned activity of the waste comes from the activation and fission products, like  $^{60}\text{Co}$ ,  $^{63}\text{Ni}$ ,  $^{55}\text{Fe}$  and  $^{137}\text{Cs}$ ,  $^{90}\text{Sr}$  and others (Vieno et al., 1998). Activation products are the products of neutron capture by the reactor structural materials. For example, the  $^{63}\text{Ni}$ ,  $^{55}\text{Fe}$  products come from the neutron activation of the steel. The nuclear fission products are the fragments, or smaller nuclei, left from the nuclear fission (Yim, 2022).

In Finland, the main sources of radioactive waste are a result of operation of the two nuclear power plants (NPPs) (Olkiluoto and Loviisa). The non-nuclear radioactive waste also can come from medical, research, and industrial applications of the radioisotopes. Posiva Oy, a jointly owned company by Fortum Power and Heat Oy (FPH) and Teollisuuden Voima Oyj (TVO) is responsible for its own waste disposal.

The reactors at Loviisa nuclear power plant went into operation in 1977 and 1981 respectively, while the construction of the Loviisa LILW repository started in 1993 (STUK, 2012). This repository is located at a depth of ~110 m in the granite bedrock. The hall-type waste caverns for solid LLW and a solidified ILW exist separately. These LLW halls are constructed with concrete floors and shotcrete walls with drainage. The waste in the drums is stacked within the tunnel and is not backfilled. The ILW hall includes a concrete basin hosting the solidified waste containers. The basin will be closed by a lid and cavern backfilled (Pitkäoja, 2019). The design of the repository at Olkiluoto differs from that of Loviisa, primarily influenced by variations in the local geological conditions. Unlike Loviisa, the Olkiluoto repository features two silos situated at a depth of 60-95 meters in tonalite bedrock. These silos are designated for solid low-level waste (LLW) and the for bituminized intermediate-level waste (ILW) respectively. Each silo is a robust concrete structure encased within the rock silo. Following the filling of the silo with concrete boxes containing bituminized waste drums, the space is subsequently backfilled with crushed rock. (STUK, 2017)

## 2.2 Disposal of low and intermediate level radioactive waste in repositories

Most of the solid waste is directly handled, packaged, and stored before disposal. If the waste can be compressed, the LLW is packaged into the drums with a hydraulic compactor. Resins, for example from ion-exchange water purification systems are dried and then mixed with cement or bitumen and packed for disposal into the drums or concrete containers. Low level waste liquids and sludges are solidified with concrete, bitumen or special solidification media directly into the disposal drum (Äikäs & Anttila, 2008). The intermediate level waste is first conditioned before storage and disposal.

During the operation of nuclear power plants (NPP), parts of the structural materials of the installation and some of the used process materials are activated by neutron absorption or contaminated with activated substances. The contaminated low and intermediate level radioactive waste (LILW) from the operation of power plants consists for example of filters, evaporator condensates and sludge from drainage waters, or maintenance waste like for example personal safety equipment and other solid process materials. When a power plant is decommissioned, additional LILW from dismantling is generated, which also needs to be deposited safely. This material includes for instance the reactor pressure vessel (RPV), pipes, valves, instrumentation, concrete from the building, or insulation materials. The steel types present in the waste include various grades of steels: carbon steels (e.g. structural material, steel barrels for waste), low-alloy steels (e.g. RPV) and stainless steels (e.g. piping, instrumentation, inner cladding of the RPV). (Nummi, 2018)

### 2.2.1 Systems involved / containers and whole reactors to be put into the repository

To ensure that radioactive substances will not contaminate the environment, LILW needs to be stored safely for a sufficiently long time in special repositories (STUK 2018, Guide YVL D.5). In Finland, the LILW will be disposed mainly in concrete containers and steel barrels into the bedrock caverns near the Finnish NPP sites. Larger activated and contaminated metallic structures, which consist mostly of carbon steels and stainless steels, will be cut into smaller pieces during the decommissioning of the NPPs. It can be expected that the steel components of the former NPPs contain welds. The cut metal pieces will be packed according to their activity in reinforced concrete containers or steel containers. These containers will be disposed to underground caverns that are excavated into the bedrock. The caverns may be equipped with additional concrete barriers. After the disposal of the LILW containers, these underground chambers may be filled by grouting depending on the waste type. (Tuunanen et al., 2014; Nummi, 2018; Tommila, 2021) Therefore, the behaviour of steel and concrete under the environmental conditions at the disposal sites is essential for the performance of the repository.

The reactor pressure vessels (RPVs) and the reactor internals to be disposed into the LILW repositories contain a large share of the radioactivity. There is an option to dispose RPVs as a whole, making it possible to dispose inside also other intermediate level radioactive waste (such as reactor internals). The pressure vessel steel of the RPV and the stainless-steel cladding on the inside of the RPV would then serve as additional release barriers. It is necessary to close the many connections of the RPV to the water circuits of the former NPP by welding stainless steel plates onto the openings. In the end, grout would be cast into the closed RPVs before they would be installed into the bedrock caverns that would further be filled with concrete. (Tommila, 2021)

### 2.2.2 Surrounding environment and its influence on the durability of the LILW containers and the safety of LILW repositories

Most of the activated and contaminated metallic waste from the operation and decommissioning of the NPPs consists of various carbon and stainless-steel grades depending on their former purpose. Carbon steel is also used for the steel containers and as reinforcement in the concrete containers and in the concrete basins or silos into which the containers will be placed. As carbon steels are often used for structural purposes in NPPs, it can be assumed that many parts contain weldments. Piping and instrumentation in the NPPs are often made from stainless steel, which typically also contains weld seams. Generally, welds between parts of the same or similar steel grades are relatively common, making them an essential part of the waste. Dissimilar welded joints between carbon steel and stainless steel are commonly rare but cannot be excluded from occurring even in NPPs.

It is reasonable to assume that most welds in equipment for the NPPs were produced under well-defined and controlled conditions resulting generally in a fairly high weld quality. Nevertheless, the metal in and around a welded joint has generally different metallurgical properties than the base materials due to its

different solidification process and a lack of thermo-mechanical treatments. It is even not uncommon that different steel phases occur in weld seams. Also, detrimental precipitates may form during cooling of weldments. It is therefore likely that weld seams have different, often more or less worse corrosion properties than the wrought base materials, which is why it is important to study the corrosion properties of the welds. Additionally, oxide layers that form during welding at high temperatures on the weld nugget and on the surfaces of the base materials can increase the risk of corrosion. Especially scale and heat tints on stainless steels can be detrimental to the corrosion resistance of the welded area. It is therefore often necessary to remove weld oxides especially from stainless steels to restore the initial corrosion resistance of the base material. Typically, this is achieved by pickling the welded area in a mixture of nitric and hydrofluoric acid, which often poses a work safety risk. In some cases, also mechanical weld cleaning methods like abrasive grinding can be applied successfully. (Kyröläinen, 1999) Therefore, it is important not only to understand the corrosion behaviour of steel sheets, but also of their weldments which are influenced by the post-weld cleaning methods.

### 2.2.3 Materials involved

One large entity to be welded is the RPV, if it is to be disposed without dismantling. RPVs are made of thick plates of pressure vessel steel, which is typically a low-alloyed Cr-Mo-V steel. The RPVs are often clad on the inside by a thinner layer of stainless-steel sheet that is corrosion resistant against the reactor water. Welding methods and quality demands for the welds that might be needed to close the openings of the RPVs with stainless steel sheets when disposing them without dismantling, have not yet been specified. It is, however, likely that the weldments could be made between the stainless-steel cladding and the stainless-steel plugs. Nevertheless, it can be expected that the surrounding outer carbon steel of the RPV would be in electrical contact with the welded stainless-steel plugs that are exposed to the outside environment. (Nummi, 2022)

## 2.3 Waters

### 2.3.1 Assumed phases of the repositories

As the waste packages will be placed into the underground disposal caverns with concrete, the presence of concrete will play a substantial role for the conditions in the repository. The concrete and grout environment at the disposal sites will be initially highly alkaline. However, the conditions will not remain the same over the whole assessment time period lasting at least 100,000 years. During the evolution of the repositories, natural groundwater will flow into the caverns of the repositories. The water at the Finnish disposal sites can be often classified as brackish Na-Cl-type groundwater (Hatanpää, 2006). As its salinity exceeds the present values of the seawater in the Baltic Sea around Finland (Pitkänen, 1996), the salt content and composition of the pore water of the concrete that is in contact with the steel parts in the LILW will change significantly over time. It is expected that the groundwater flow into the repository will lead to a slow degradation of the concrete, for instance by erosion, leaching and chemical reactions with chemical compounds in the groundwater, like sulphate or carbonates. The chlorides in the groundwater may also attack steel reinforcements. Together with the formation of carbon dioxide from the possible decomposition of organic waste in some areas of the repositories, the groundwater will neutralize the alkaline concrete porewater over time, so that the initial high pH value of around 12-13 will eventually settle to neutral values of around 7 (Kari, 2014).

It is assumed that the risk for corrosion of the steel parts in the repository will be initially suppressed by the high pH value of the alkaline grout and concrete environment ensuring their chemical stability (Winston, Revie and Uhlig, 2008). The uniform corrosion rates of carbon steels will be very low and localized corrosion of stainless steel, like for instance chloride-induced pitting, will be unlikely (Ahlström, 2015). The alkaline environment will also help to immobilize radioactive transition metal cations by solid precipitate formation, so that they won't pass easily into the environment for some time (Tandré, 2020). These positive

effects of the alkaline concrete will persist for some time even after saline groundwater has entered the underground disposal site. But as the porewater in the concrete will be neutralized gradually to lower pH due to contact with the steel waste, the aggressiveness of the environment towards carbon and stainless-steel waste will increase (Rajala, 2017). At some point of the neutralizing process, the uniform corrosion of carbon steel will become more pronounced, which could also lead to an increased hydrogen gas formation due to the predominant cathodic reaction of the corrosion processes in anoxic environments (Huang, 2021). Additionally, over time, the increasing chloride content in the water that is in direct contact with stainless steel parts will raise the risk for localized corrosion, like pitting and crevice corrosion. Nevertheless, the probability of localized corrosion will only increase slightly due to the low redox potential of the environment, that is assumed to remain anoxic. Similarly, the relatively low temperatures at the disposal site can slow down or even hinder completely corrosion process of carbon and stainless steels. (Sedriks, 1996) All in all, there are several processes taking place and affecting the conditions present in the repository, thus also affecting the corrosion system.

### 2.3.2 Pore water

Cement has many favourable properties, both chemical and physical, making it a desirable barrier or matrix for the encapsulation of radioactive and toxic wastes. Chemically, cement has a high pH (e.g. its pore water) and forms hydration products which favour sorption and ion substitution. Physically, cement is a durable solid material with a low permeability in its hardened state which protects the radioactive waste, facilitating its safe transportation and storage. Cement is also an inexpensive and readily available material, durable in its hardened state, fluid when initially cast and tolerant to a variety of waste forms, including those in solid and liquid states. Cements have also been proved to show their stability when irradiated and ability to act as radiation shielding. Conventional cementitious materials such as ordinary Portland cement (OPC) and OPC-based composite cements, as well as novel cement systems can be used to create reliable immobilizing elements for safe storage and disposal of wastes. These barriers function, as well as interactions envisaged between various components, were considered in this CRP which was focused on predisposal management systems.

In a chemical approach to cementitious materials degradation under simple leaching conditions, four states of the evolution of cement are suggested for benchmarking. These stages are achieved by sacrificial dissolution of cement substance and are summarized as follows (Glasser, 2011): (1) Stage I: The pH is dominated by alkalis: all normal cement mineral hydrates are present. (2) Stage II: The pH is dominated by  $\text{Ca}(\text{OH})_2$ : all normal hydrates are present. (3) Stage III:  $\text{Ca}(\text{OH})_2$  is consumed: pH is buffered in the range 10–12. (4) Stage IV: Only degradation and reaction products are left to condition pH. The main cations in the cement pore water are Na, K, and Ca. The four-stage approach is used in performance assessments for radioactive waste repositories for geochemical modelling of cementitious barrier durability with respect to providing chemical buffering for radionuclide phases and physical/hydraulic durability (porosity, permeability and tortuosity) of the matrix portion of the barrier.

### 2.3.3 Groundwaters (+ Differences in sites)

The Loviisa NPP is located on the Hättholmen research site 13 km SSW from the town of Loviisa (Hatanpää, 2006). The bedrock at the site is composed of rapakivi granite and is Precambrian in age. The Olkiluoto repository is on the west side of the Olkiluoto island (Pitkanen et al., 1999). The bedrock surrounding the Olkiluoto site is also Precambrian in age and comprised of rapakivi granite. The rock chemistry of the Loviisa area is rich in iron and potassium, and poor in aluminium. In comparison to the Loviisa site, the Olkiluoto rock composition varies in terms of the main rock types present. Pyterlites of Loviisa is low in sulfur, but rich in chlorine. The mafic gneisses in Olkiluoto are, on the other hand, rich in sulfur and contain low amounts of chlorine.

The groundwater-types at Loviisa have similar characteristics to those found at Olkiluoto (Pitkänen et al., 1998). Fresh groundwater is limited at both sites to the upper part of the bedrock. Brackish groundwater

with total dissolved solids (TDS) ranging from 2 000-9 800 mg/l has been observed at both sites. The TDS increases with depth, and therefore at larger depths, the water is more saline, however the enrichment of TDS is varies with depth (the ions majorly present in water). For instance in the Loviisa NPP grounds, the dilute Ca-Na-Mg-HCO<sub>3</sub>-(SO<sub>4</sub>)-(Cl)-type water is present at depths to 60 m. At depth ranges of 60–600 m SO<sub>4</sub>-rich brackish Na-(Ca)-Cl type groundwater is found, while at depth deeper than 600 m – saline Na-Ca-Cl groundwater. The Olkiluoto groundwater changes with depth with the fresh but slightly brackish Na-Cl-HCO<sub>3</sub>-type water at 0–150 m to brackish Na-Cl-(SO<sub>4</sub>) water at 150–500 m, and saline Ca-Na-Cl groundwater at the depths more than 500 m.

In the Olkiluoto groundwater, chloride (Cl<sup>-</sup>) is the most abundant anion. As the depth increases, the amount of Cl also increases. The main anions that contribute to the total alkalinity are HCO<sub>3</sub>+CO<sub>3</sub>, and the total alkalinity decreases with increasing depth. Notably, as the chloride amount increases, alkalinity values decrease from the precipitation of calcite, which already may precipitate at shallow depth at Olkiluoto. As for the cations, the calcium concentrations increase with depth with chloride. All groundwaters in Olkiluoto are highly enriched with calcium compared to the sea water. Magnesium shows a different behaviour, with waters being very depleted in Mg compared to the sea water. According to Pitkänen et al. (1994; 1996), the Mg contents are enriched in the brackish sulphate-rich groundwater at depths of approximately 100-300 m. Potassium, similarly to magnesium, mainly enriches waters at the depths of 100-300 m, but there is a generally smaller concentration of K compared to Mg.

The Loviisa groundwater also shows an increase in chloride amounts with increasing depths. However, compared to Olkiluoto, there is considerably more Cl<sup>-</sup> dissolved in the water. The main cations in Loviisa groundwater show a general increasing trend with increasing concentration of chloride, and thus depth. This for both Loviisa and Olkiluoto groundwater reflects the various water-rock interactions and mixing.

Overall, the water collected near the surface (< 100 m) is characterized by low Cl (< 20 mg/l), as depth increases (100-300 m), brackish water contains moderate Cl levels of approximately 2500-5300 mg/l. At depths 600-1000 m the groundwater is saline with Cl levels ranging from 10000 mg/l to ~30000 mg/l. The total alkalinity similarly decreases with increasing depth. The observed maximum alkalinity is observed at depths of 20-50 m at 3.8 meq/l in Loviisa groundwater. For Olkiluoto, fresh groundwater also showed maximum alkalinity values of ~7 meq/l at the similar depth range. Both show high values due to the influence of atmospheric and biogenic CO<sub>2</sub>. At large depths, the total alkalinity of Loviisa and Olkiluoto groundwaters can be as low as 0.5 and 0.1 meq/l respectively (Hatanpää, 2006; Pitkanen et al., 1999).

The dissolved gases in the groundwater similar to the ions increase with depth. Main gases detected in the water are methane, hydrogen, sulfur-containing gases, and higher hydrocarbons (Lampen & Snellman 1993, Snellman et al. 1995a, Ruotsalainen & Snellman 1996).

In the case with the redox conditions and pH of the groundwaters, there is a clear trend of increasing pH with depth and, as mentioned, greater salinity of the groundwater. The lowest pH values are commonly observed at shallow depths. The pH values of deep borehole groundwaters at Olkiluoto range from 7.3 to 9.0 and at Loviisa 7 to 8. The initial increases in alkalinity and pH is generally interpreted as mainly resulting from fracture calcite dissolution in CO<sub>2</sub>-rich recharge water (Nordstrom et al., 1989). A similar interpretation is considered to be valid for HCO<sub>3</sub>-rich groundwater at Loviisa.

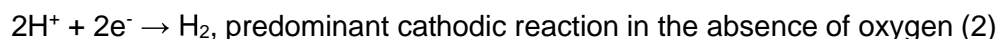
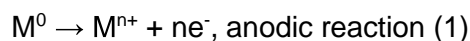
The measured redox values (E<sub>h</sub>(Pt)) refer to slightly or clearly reducing conditions for most of the brackish and saline groundwater samples. The brackish groundwater has the largest range of E<sub>h</sub> values from about +30 to -340 mV and the saline groundwater has a bit higher range, +9 to -230 mV in Loviisa groundwater samples. A general feature of measured E<sub>h</sub>(Pt) at Olkiluoto and Loviisa is that the most frequent observations of low, reducing conditions have been made in saline groundwater samples and with increasing pH. (Hatanpää, 2006; Pitkanen et al., 1999)

The contents of total iron ( $\text{Fe}_{\text{tot}}$ ) and ferrous iron ( $\text{Fe}^{2+}$ ) both increase with depth in the saline groundwaters. The median value of  $\text{Fe}_{\text{tot}}$  in the Olkiluoto groundwaters was  $3.0 \times 10^{-3}$  mmol/l compared with the theoretical lower limit ( $10^{-3}$  mmol/l) of iron for successful Eh measurements, if  $\text{Fe}^{2+}/\text{Fe}^{3+}$  is the redox controlling couple (Grenthe et al., 1992). However, according to previous evaluations (Pitkänen et al., 1996) sulphur species play the most important role in controlling redox conditions at Olkiluoto (Pitkänen et al., 1996). Total sulphide values ( $\text{S}^{2-}_{\text{tot}} = \text{H}_2\text{S} + \text{HS}^- + \text{S}^{2-} + \text{polysulphides}$ ) show a general trend of elevated  $\text{S}^{2-}_{\text{tot}}$  content mostly among samples from 250 – 500m depth suggesting microbially catalysed  $\text{SO}_4$  reduction. This is in good agreement with the results of microbes showing a large amount of sulfate reducing bacteria (SRB) at these depths in Olkiluoto and Loviisa groundwaters (Haveman et al., 1998).

Redox conditions in the Loviisa saline groundwater layer are clearly dominated by iron oxyhydroxides and dissolved iron in the groundwater. However, the calculated redox values suggest that the system has reached the sulphidic condition. In relation to the redox conditions, the pH level in saline groundwater is somewhat lower at Loviisa (around 7.5) than in Olkiluoto (likely above 7.5). The pH for the Loviisa deep groundwater will remain at a low level due to the very poor solubility limit for iron and the hydroxyl complexation of it. The predicted Eh range is  $-200 \pm 50$  mV at Loviisa whereas it is  $-250 \pm 50$  mV at Olkiluoto.

## 2.4 Corrosion and its affecting factors

Corrosion is the destructive attack of a metal by chemical or electrochemical reaction with its environment. Electrochemical corrosion is a chemical reaction involving the transfer of electrons from the zero-valent metal to an external electron acceptor, causing the release of the metal ions into the surrounding medium and the deterioration of the metal (Equations 1 & 2).



There are four basic requirements for corrosion to occur. Among them is the anode, where dissolution of metal occurs, generating metal ions and electrons. These electrons generated at the anode travel to the cathode via an electronic path through the metal, and eventually they are used up at the cathode for the reduction of positively charged ions. These positively charged ions move from the anode to the cathode by an ionic current path. Thus, the current flows from the anode to the cathode by an ionic current path and from the cathode to the anode by an electronic path, thereby completing the associated electrical circuit. Anode and cathode reactions occur simultaneously and at the same rate for this electrical circuit to function.

The five main types of corrosion classified with respect to outward appearance or altered physical properties are as follows (Revie, 2011):

1. General Corrosion, or Uniform Attack. This type of corrosion includes the commonly recognized rusting of iron or tarnishing of silver. "Fogging" of nickel and high - temperature oxidation of metals are also examples of this type. Generally, for uniform attack, the initial corrosion rate is greater than subsequent rates. Duration of exposure should always be given when corrosion rates are reported because it is often not reliable to extrapolate a reported rate to times of exposure far exceeding the test period.
2. Pitting. This is a localized type of attack, with the rate of corrosion being greater in some areas than in others. If an appreciable attack is confined to a relatively small, fixed area of metal, acting as anode, the resultant pits are described as deep. If the area of attack is relatively larger and not so deep, the pits are called shallow.
3. Intergranular Corrosion. This is a localized type of attack at the grain boundaries of a metal, resulting in loss of strength and ductility. Grain – boundary material of limited area, acting as anode, is in contact with large areas of grain acting as cathode. The attack is often rapid, penetrating deeply into the metal and sometimes causing catastrophic failures.

4. Dealloying, Dezincification, and Parting. Dealloying is the selective removal of an element from an alloy by corrosion. Parting is similar to dezincification in that one or more reactive components of the alloy corrode preferentially, leaving a porous residue that may retain the original shape of the alloy.
5. Stress corrosion cracking. If a metal cracks when subjected to repeated or alternate tensile stresses in a corrosive environment, it is said to fail by corrosion fatigue.
6. Hydrogen embrittlement. Hydrogen embrittlement is the process by which metals such as steel become brittle and fracture due to the diffusion of hydrogen into the metal (Winston, Revie and Uhlig, 2008). Hydrogen embrittlement may also be linked to the evolution of SCC. In many cases, the critical hydrogen concentration that can lead to failure of a sensitive material is low.

Carbon steel is the most easily corroding component of radioactive metal waste. The possible corrosion processes in the repository conditions can be predicted based on the potential-pH diagram of iron (Figure 1). Based on the Pourbaix diagram, if the potential of iron is more negative than -1100 mV on SHE (standard hydrogen electrode) scale metallic iron is stable across the whole pH range (0-16). In practice, the potential of an iron sample in water solution is between -400 ... -800 mV, and so the corrosion can occur with three different reactions depending on the pH. First, a passive oxide layer formation is anticipated. However, this film does not stop the corrosion, only the corrosion rates are reduced. The maintenance of the passive film requires both a high pH (>9) and excess of oxygen. In final repository conditions, the availability of oxygen is limited and thus all of the oxygen in the concrete may be reduced by the slow corrosion reaction. However, due to the radioactive nature of the waste, the radiolysis of water at the metal surface inside the concrete container can create oxidizing conditions (Preece, 1982).

If all the oxygen is consumed, the potential drops and the passive oxide layer becomes unstable and reduces. The corrosion rate of the steel in this 'active' state is determined by the potential, the diffusion rates of the reactants and the corrosion products and the resistivity of the surroundings (Preece, 1982).

The most important on affecting the corrosion properties of steels is chloride, which is always present in the groundwater.

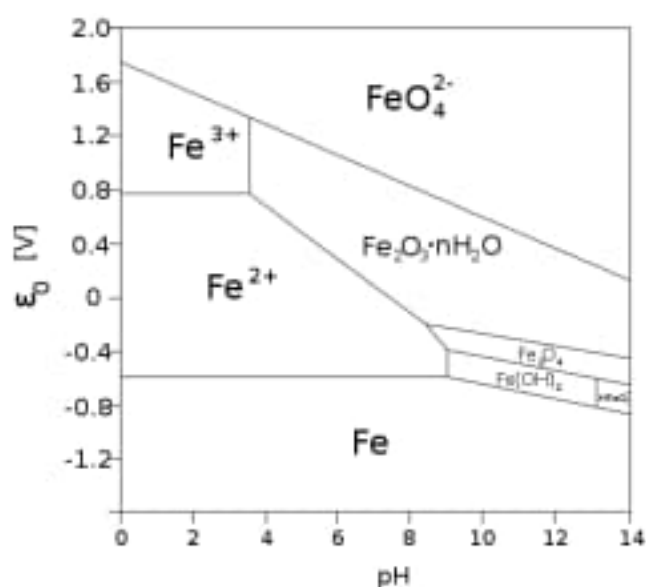


Figure 1. Pourbaix diagram of Iron-Water system;  $c(\text{Fe}) = 10^{-6} \text{ mol/l}$ ,  $T = 25 \text{ }^\circ\text{C}$  (CC BY-SA 2.5).

Stainless steels are iron-base alloys containing chromium and usually also nickel. The corrosion of iron was discussed above, and to understand corrosion of stainless steel the corrosion mechanisms of nickel and chromium will be described. Corrosion rates of nickel in its alloys are slower than that of iron alloys in almost any conditions. Generally, oxidizing conditions favour the corrosion of Ni, but nickel can protect

itself with a passive oxide layer. If the oxide layer is locally destroyed, however, pitting corrosion may occur. The corrosion rates of nickel alloys are expected to be low. However, high local concentration of chlorine ions may cause the protective layer breakdown, similar to iron, causing pitting corrosion. Nickel is also a good electrode for hydrogen formation and local corrosion at highly alkaline conditions may lead to the formation of hydrogen.

The passivity area of chromium extends over a wide area of pH at low potentials. In stainless steels, the good corrosion properties are mainly based on the passive film formed by chromium oxides. Thus, chloride ions increase the risk of corrosion of stainless steel, especially when local corrosion processes are enhanced in the presence of chloride, similar to Fe and Ni.

Corrosion can increase the rate of material degradation thus shortening the time during which the barriers work properly. Typically, corrosion rates and compound transport are very low due to the high pH in environments including concrete. However, the erosion of concrete and the flow of groundwater into the concrete barriers and waste packaging can expose the waste to various corrosion mechanisms (Lane, 2005). Steel corrosion can be limited in the high alkalinity due to formed passive layers (Winston, Revie and Uhlig, 2008). In addition, it was shown that concrete has an inhibiting effect on corrosion at least at the beginning of the repository life span and limits the occurring microbe types to alkaliphilic bacterial groups (Rajala et al., 2016, Rajala 2017). The concrete casings form a protective barrier hindering the activities of microorganisms as long as they are intact maintaining the high alkaline pH and high carbonate concentration in the repository environment (Pedersen 1999, Rajala et al., 2016, Rajala 2017, Rajala et al., 2017). However, there are implications that microbial activity can also affect the concrete barrier performance by locally lowering the pH already after four years (Small et al., 2008) thus having a negative effect on the overall durability of the whole disposal system. As a nuclear waste repository must be able to prevent the release of radionuclides for a long time it is necessary to study the impact of deep groundwater containing microorganisms on welded structures in a scenario where the concrete has aged and deteriorated so that deep groundwater is already passing to the steel structures and weldments.

#### 2.4.1 MIC-related occurrences and previous findings

The deterioration of metals or metal alloys generated by microbial activity is termed microbially induced corrosion, microbiologically influenced corrosion or biocorrosion (MIC). The electrochemical nature of corrosion remains valid also for MIC. The participation of microorganisms in the process induces several effects, the most significant being local changes in the electrochemistry at the metal-solution interface under the microbial biofilm (Videla et al., 2005). MIC is not one distinct type of corrosion, but the term is used to designate corrosion resulting from the microbial metabolism of the metal surface biofilms or close to the surface. MIC is a result of interactions between the metal surface, abiotic corrosion products, and microbial cells and their metabolites (Beech et al., 2004). In most cases, MIC occurs as a localized corrosion that results in pitting, selective leaching, crevice corrosion, under deposit corrosion, or erosion corrosion (Little et al., 1992).

Subsurface groundwaters are likely to transport microbes within fractured bedrock. When the repositories evolve and aged concrete no longer maintains the inhibiting high pH, newly transported microbial cells will be introduced from the groundwater to the steel surfaces in the LILW. Stainless steel, carbon steel and welds in the LILW containers are then likely affected by biofilm formation, microbe-metal interactions, potential corrosion processes, and gas production (Small & Vikman, 2020). Microbial colonies can contain micro-niches with varying environmental conditions formed for example under the biofilm and the EPS layers. Damage caused by corrosion may generate a risk to the durability of the containers and their welds, and there is still insufficient data to understand or model MIC in different repository environments (Černoušek et al., 2020).

There is increasing information available on MIC in the welded joints, for example, in oil pipes (Liduino et al., 2019), or in cooling and/or sprinkler systems circulating either fresh or sea water (Carpén 2008, Yasuyuki et al., 2002), but there is rare information available regarding the corrosion resistance or behaviour of welded joints in contact with anoxic saline or brackish subsurface groundwaters. In other environments, it has been shown that MIC especially affects steel surface areas with welded joints (Liduino et al., 2019, Anzai et al., 2006), but welds and their microbial communities remain less represented in research. In marine environments, welded steel surfaces have reported higher corrosion rates compared to non-welded ones, and stagnant water increases corrosion rates compared to turbulent water flow (Liduino et al., 2019). In marine microcosms, steel surfaces and two different weld types were shown to host different microbial communities (Garcia & Procópio 2020). This phenomenon could be due to different surface roughness properties providing better sites for microbial adherence or the welds having oxidized steel surfaces could contain different overall compositions than other steel surfaces, for example higher levels of manganese oxides. Higher manganese content at the welds could thus favour the actions of manganese cycling microbes related to the oxidation and reduction of manganese. Microbially mediated manganese oxidation and reduction are considered relevant in other environments as deposited manganese oxides on steel surfaces may promote corrosion (Beech & Sunner 2004, Linhardt 2010).

Microbial activities within the steel surface biofilms, and potentially also weld biofilms, can be linked to multiple key biogeochemical cycles including sulfur, nitrogen, and manganese cycles (e.g., Rajala 2017). Especially the SRBs have been deemed important for microbially influenced corrosion (MIC) in anoxic repository conditions, as they potentially interact with the steel surfaces by transferring electrons or by producing corrosive metabolites or deposits during sulfate reduction (Urios et al., 2014, Li et al., 2018, Rajala 2017). In addition to facilitating better microbe-metal interaction, biofilms also enable microbe-microbe interaction which can be crucial in oligotrophic environments. To our best knowledge, there are very few studies on the microbial community composition or their MIC-related roles on weld surfaces in the LILW repository conditions.

#### 2.4.2 Microbiology related to the LILW repositories

One factor affecting the evolution of the repositories is the microbial activity. Repository environments are not isolated and interact with their surrounding biospheres and geospheres during their evolution. Microorganisms present in the Fennoscandian subsurface groundwaters and inhabit the surfaces of bedrock fractures and crevices as biofilms or as attached small colonies (Pedersen 2013; Purkamo et al., 2016, Bomberg et al., 2016; Nuppunen-Puputti et al., 2020; Nuppunen-Puputti et al., 2022; Somervuori et al., 2021; Bell et al., 2020). The composition of the groundwater as well as the planktic microbial community compositions tend to fluctuate (Rajala et al., 2022).

In the Olkiluoto repository site, the formed steel surface biofilms were shown to be unevenly distributed and focused on the materials grain boundaries after a two-year *in-situ* contact with groundwater (Rajala et al., 2022). The microbes in the formed biofilms differed from the planktic groundwater microbial communities which also changed over time (Rajala et al., 2022). The most common orders in the two studied drillholes (A and B) were *Campylobacteriales* and *Desulfobacteriales* - a consortium of sulphate-reducing bacteria (SRB). In addition to SRB, sulfur oxidizing bacteria, such as *Sulfuricurvum*, were observed in drillhole B. Furthermore, also archaea such as *Methanosarcinales* had attached to the steel surfaces. Despite the previous assumptions on groundwater stability, it was suggested that there are fluctuations of both the deep groundwaters and its microbiome which could have impacts on the evaluation of the repository's stability and safety. The sulfur-cycling microbes could potentially enable better groundwater contact with steel materials by enhancing local disruptions of the passive layer thus further enhancing the detrimental effects of chloride dissolved in the groundwater (Rajala et al., 2022).

Metagenomic data from rock surfaces obtained from the Outokumpu deep borehole indicated that rock surface microbiomes host different genes related to manganese cycling, especially for the transport of



manganese (Nuppunen-Puputti et al., 2022). Genes for both manganese oxidase (*mcoA*) and manganese-oxidizing peroxidase (*mopA*) were observed in bacterial metagenome-assembled genomes (MAGs) (Nuppunen-Puputti et al., 2022). The microbial anaerobic manganese cycle has an interesting role as it couples multiple relevant biogeochemical pathways (Wang et al., 2022). In anaerobic conditions that will prevail later during the repository evolution, manganese could facilitate critical biogeochemical cycles linked to ammonium oxidation, sulfide oxidation, methane oxidation (ANME) as well as organic carbon oxidation (Wang et al., 2022).

### 3. Materials and methods

---

#### 3.1 Materials

##### 3.1.1 Steels

###### 3.1.1.1 Fe 37 B

The carbon steel used for the tests was denoted as Fe 37B. Its surfaces were machined before the welding. The thickness of the material was 14-16 mm. For welding, it was water jet cut into approximately 1000\*150 mm pieces. OES analysis by Eurofins (see Appendix) showed that it had Mn and C as its main alloying elements, with small quantities of other elements including Si, Cu, Nb and Ni.

###### 3.1.1.2 Pressure vessel steel

The pressure vessel steel (PVS) was authentic steel obtained from a previous project on welding of pressure vessel steel. It was received as a larger block with the dimensions of approximately 190\*115 mm, and approximately 110 mm height of material underneath the weld. This part was then cut to seven ca. 190\*115 mm plates machined from both sides with a final thickness of approximately 8 mm for the welding tests, and three ca. 190\*115 mm plates of approximately 3 mm final thickness machined from one side for the initial baseline electrochemical tests. Prior to welding, the surface was washed with Eko Puhto detergent, and subsequently rinsed with water and 70% ethanol to remove grease and dirt.

###### 3.1.1.3 321

Stainless steel 321 (EN 1.454) was obtained as 1000\*100 mm waterjet cut pieces with the thickness of 8 mm for the welding tests. Prior to welding, the surface was washed with Eko Puhto detergent, and subsequently rinsed with water and 70% ethanol to remove grease and dirt. For the initial baseline electrochemical tests, 321 with a thickness of 2 mm was used. For the electrochemical measurements the surfaces were grinded to 500 grits, washed with ethanol and dried thoroughly.

###### 3.1.1.4 316L

Stainless steel 316L (EN 1.4404) was used as pieces with a minimum width of 95 mm and minimum length of 210 mm. Thicknesses of 10 mm and 6 mm were used for the welding tests and 6 mm for the baseline electrochemical tests. The surface was also grinded to 500 grits for the electrochemical measurements and treated in the same manner. The surface condition of the steel was 1D. Prior to welding, the surface was washed with Eko Puhto detergent, and subsequently rinsed with water and 70% ethanol to remove grease and dirt.

### 3.1.2 Welded steels

Altogether four types of welds were manufactured at the Taitotalo premises. The detailed parameters of the welds are presented in section 3.2.1. Figure 2a-d show the images of the types of manufactured welds.

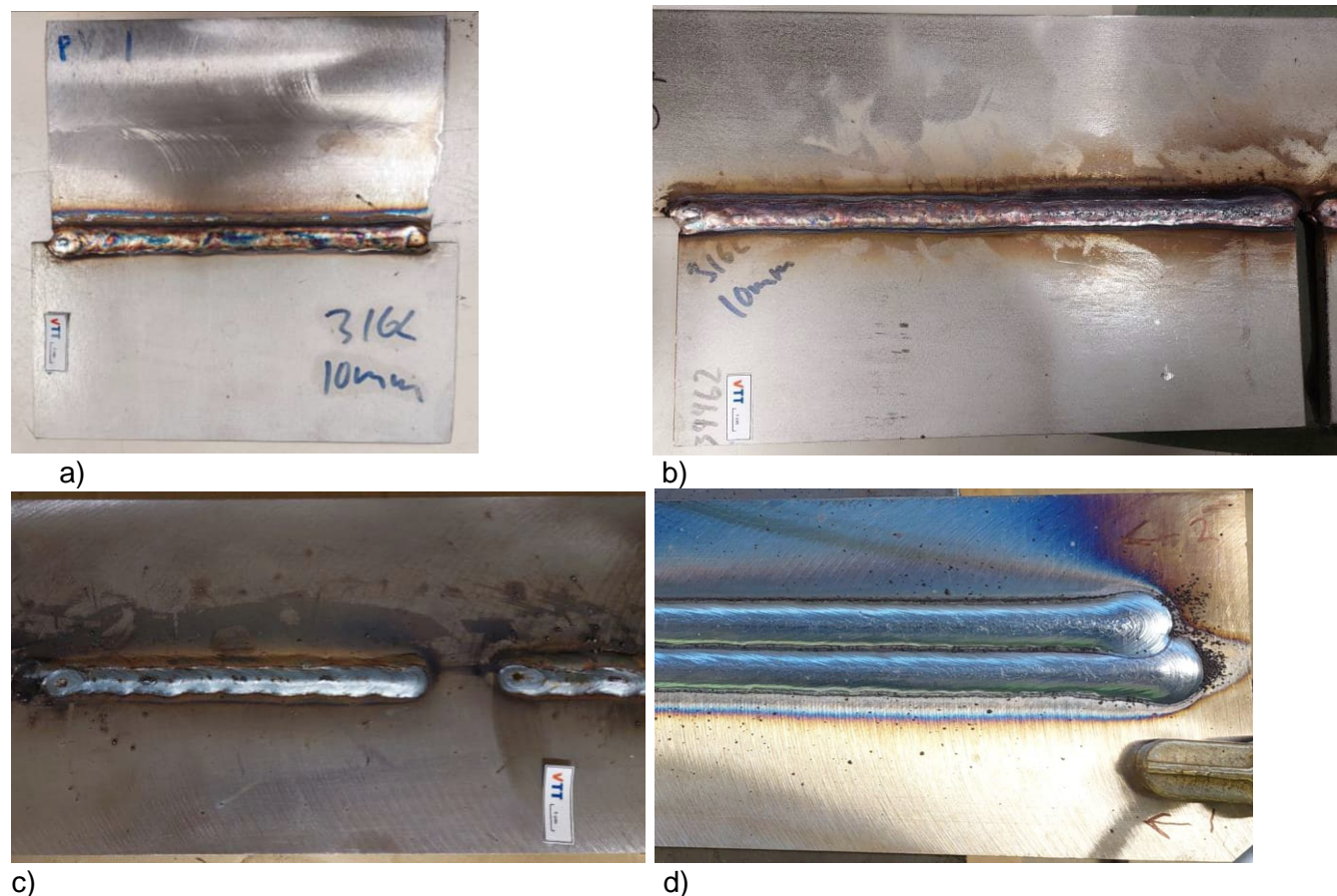


Figure 2. The welds produced by gas-metal-arc welds for a) PVS-316L, b) 321-316L and bead-on-plate welded Fe 37B samples with c) gas-metal-arc welding and d) submerged-arc welding.

### 3.1.3 Waters

#### 3.1.3.1 Simulated concrete pore water (CPW)

Simple alkaline solutions simulating concrete pore solutions were used for steel corrosion testing. In this work, concrete pore solution was simulated by a solution of NaOH, KOH, and Ca(OH)<sub>2</sub> mixtures (15.8 g/L, 37.3 g/L, and 0.178 g/L respectively) with pH 14, which was prepared with analytical grade reagents and Milli-Q water. The diluted CPW samples were prepared by diluting the CPW (pH 14) with Milli-Q water to obtain solutions with pH 10 and 8. The pH 7 solution is represented by pure Milli-Q water. The prepared samples are then specified as CPW1 (pH 14), CPW3 (pH 10), CPW5 (pH 8), and CPWDI (pH 7).

#### 3.1.3.2 Simulated ground waters (GW)

The compositions of the artificial groundwaters used in the experiments are shown in Table 1. The salt content of the groundwaters is based on the ionic composition of the groundwater at ~100m reported in the hydrogeochemical reports (Luukkonen et al., 1999, Pitkänen et al., 1998). All chemicals were analytical grade and solutions were prepared using Milli-Q water. To reach the groundwater pH, 1M NaOH was added. The pure simulated groundwater was diluted with the CPW to obtain pH 8 and 10. To reach anoxic

environment, argon (Ar) was used for deoxygenating the groundwater by bubbling the water in storage bottles for 30 minutes and then bubbling Ar in the cell for 20 minutes prior to the measurements. In case of precipitate formation, simulated groundwaters are mixed overnight under argon atmosphere. The samples are then referred as GW3-L (pH 10), GW5-L (pH 8), and GW-L

Table 1. Simulated groundwater composition for tests.

	Loviisa Simulated Groundwater (g/L)	Olkiluoto Simulated Groundwater (g/L)
NaCl	3.96	1.22
Na <sub>2</sub> SO <sub>4</sub>	0.56	0.23
KCl	0.044	0.008
NaHCO <sub>3</sub>	0.134	0.432
KBr	0.024	0.0052
KF	0.003	0.0015
CaCl <sub>2</sub> · 2H <sub>2</sub> O	2.255	0.248
MgCl <sub>2</sub> · 6H <sub>2</sub> O	2.257	0.251
Na <sub>2</sub> SiO <sub>3</sub> · 9H <sub>2</sub> O	0.052	0.032

## 3.2 Methods

### 3.2.1 Welding

Two arc-welding processes, submerged-arc welding (SAW) and gas-metal-arc welding (GMAW, i.e., MIG/MAG) were chosen for the preparation of the welded corrosion test samples. These processes are commonly applied for the welding of RPV and NPP components. SAW process is well-suited particularly for welding long, continuous seams as multiple-pass mechanised welding of thick-wall sections, as is the case with RPVs. GMAW process, in turn, is more versatile and can be applied either as manual or automated to all-position welds over a wide range of section thicknesses and for joining dissimilar metals, as well.

#### 3.2.1.1 SAW

Experimental samples using SAW were made as bead-on-plate welds on plain carbon steel (Fe37B), representing weld filling and cap beads in an authentic structure/repository container exposed to corrosive media. On each sample, two parallel weld beads were deposited using DC+ current mode. As welding materials, unalloyed low-carbon, medium-Mn, low-Si general purpose SAW wire OE-S2 (3.2mm; AWS A5.17: EM12K; EN ISO 14171-A: S2) was applied in the combination of an agglomerated rutile-type OP 191 flux (EN ISO 14174: SA AR 1 87 AC) with low basicity index (Boniszewski: 0.4) and intended for welding general structural steels. The applied welding parameters for the SAW bead-on-plate test welds are given in Table 2.

Table 2. The applied welding parameters for the SAW bead-on-plate test welds.

Process/ Parameters	Welding current range I (A)	Arc voltage range E (V)	Torch travel speed v (cm/min)	Heat input Q (kJ/mm)
SAW: OE-2 (3.2 mm) / OP 191	575 - 580	31 - 32	44.5	2.4 – 2.5

\*) heat input calculated acc. to SFS-EN 1011-1

### 3.2.1.2 MIG/MAG

Experimental samples using GMAW (MAG) were made both as multipass (i) bead-on-plate welds and (ii) multipass butt-welds into a square-I-groove with a minimal root gap and no root face. As base materials, four different steel types: plain carbon steel (Fe37B), low-alloy (HSLA) pressure vessel steel, extra-low carbon 'acid-proof' austenitic stainless steel 316L and titanium-stabilised austenitic stainless steel 321 were applied. For plain carbon steel, two parallel weld beads were deposited as bead-on-plate welds, whereas for the rest of the materials, one weld bead was made into the square-I-groove on the top surface and an additional root pass onto the reverse side to fully close the gap (as no full-penetration was achieved). As welding materials, un-alloyed C-Mn-Si-type OK Autrod 12.51 solid wire (1.0mm; SFA/AWS A5.18 : ER70S-6 / EN ISO 14341-A: G 3Si1), 308-type 12150-N-B308LP rutile flux-cored filler wire DW-308LP (1.2mm; AWS A5.22 E308LT1-1/4) with 'matching' chemical composition and an over-alloyed 23/24%Cr-12/13%Ni 309MoL-type 12150-N-B309MoLP rutile flux-cored filler wire DW-309MoLP (1.2mm; AWS A5.22 E309LMoT1-1/4), were used. Of these, the last one was used for welding dissimilar weld joints between a low-alloy (HSLA) pressure vessel steel and the austenitic stainless steel. For all filler materials, an Ar-25%CO<sub>2</sub> mixture shielding gas was applied. The applied welding parameters for GMAW (MAG) test butt-welds are given in Table 3.

Table 3. The applied welding parameters for GMAW (MAG) test welds.

Process/ Parameters	Welding current range I (A)	Arc voltage range E (V)	Torch travel speed v (cm/min)	Heat input Q (kJ/mm)
MAG: OK12.51 (1.0 mm)	190 – 205 230 – 240	23.5 – 24.8 27.2 – 27.9	45 – 60	0.48 – 0.55 0.50 – 0.54
MAG: DW- 309MoLP (1.2 mm)	230 - 240	26	50.4	0.57 – 0.60
MAG: DW-308LP (1.2 mm)	250 - 260	28.8 - 29	45 – 60	0.60 – 0.77

\*) heat input calculated acc. to SFS-EN 1011-1

### 3.2.2 Electrochemical methods

For evaluation of the corrosion behaviour of welded sites, first baseline measurements of bulk metals were performed. Open circuit potential (OCP) recording and potentiodynamic polarization (PDP) measurements were performed. For these measurements, specimens of carbon steel (Fe 37 B – 4 x 4 x 1.4 cm) and stainless steels (316L- 3 x 3 x 0.6 cm and 321- 3 x 3 x 0.2 cm). Avesta cell was used with the exposed working electrode area of 3.14 cm<sup>2</sup>, maintaining the temperature of 22 °C for the measurements. Platinum wire was the counter electrode, and a saturated Ag/AgCl electrode was the reference electrode in the measurements. Reference electrode potential is checked before every measurement. Prior to PDP measurements, OCP records were collected for 30 minutes. PDP measurements were performed from -500 mV and +1500 mV with respect to OCP using the scan rate of 0.333 mV s<sup>-1</sup>. The measurements were carried out using a Gamry Instruments potentiostat Reference 600-21031. Tafel slopes, and corrosion rates were calculated in Echem Analyst 2 (v 7.10.1.13238) software.

### 3.2.3 Optical microscopy

After the electrochemical experiments, the samples were observed under a stereomicroscope Zeiss Axio Zoom.V16.



### 3.2.4 Microbiological methods

#### 3.2.4.1 Sampling of groundwaters from Loviisa (PLVA5) and Olkiluoto (VLJ-KR9)

Two individual sampling campaigns for deep groundwater from the Loviisa (PLVA5) and Olkiluoto (VLJ-KR9) repository sites were performed during spring-summer 2023. Prior to the microbiological sampling both sampled drillholes were flushed/purged over 3-4 weeks. The field measurements performed on site included: pH, oxygen, redox, and electrical conductivity (EC).

##### 3.2.4.1.1 Water chemistry

One set of water samples was collected from each drillhole to the ALS global water sample bottles (50-500 mL in volume) in accordance with the manufacturer's instructions. Sulfide samples (125mL) were preserved on site with the ZnAc that was readily deposited in sample bottles. Fe<sup>2+</sup> samples (60 mL) were preserved prior to analysis with HCl readily in the sampling bottles. Samples for DOC analyses were filtered with a syringe through a 0.45 μm pore-sized polyethersulfone (PES) filter to the sample bottle. The water samples were stored in a cold box and sent to ALS Global on the following day. Samples were analysed in ALS within five days.

##### 3.2.4.1.2 Water microbiology

Microbiological samples were collected in sterile and anaerobic Schott bottles, which were acid-washed and autoclaved in N<sub>2</sub> atmosphere. The bottles were capped with 2 cm-thick black butyl rubber corks (Glasgerätebau Ochs, catalogue no. 444704), and samples were collected with a needle technique through sterile tubes, needles, and corks to minimize any oxygen contamination during sampling. Samples were kept in the cold box (< 8°C) until transport to the laboratory. In the laboratory, the microbiological samples were filtered onto cellulose acetate filters (CA, 0.22μm pore-size, Corning) in triplicates (3 × 1000 mL). In addition, triplicates (3 × 5000 mL) of metagenomic water samples were collected on filters. For both volumes, the filters were cut out from the cups with a sterile scalpel, placed onto sterile 50mL Corning tubes, and kept frozen at -80°C until further handling. Duplicate 10 mL water samples were fixed in 15% glycerol overnight at 4°C for the DAPI enumeration of microbial cell counts.

DAPI (2.5 mg/mL, 4',6'-diamidino-2-phenylindole, SIGMA D9542) was diluted to 0.5 mg/mL using sterilized 25% glutaraldehyde (GTA, Merck 820603). The fixed water samples were then stained with diluted DAPI at room temperature and in a dark place for 20 minutes. After that, the microbial cells were collected by filtering the water samples through 0.2 μm filters (Millipore GTBP02500). Each filter was aseptically placed onto a 76 x 50 mm microscope slide (Thermo Scientific), mounted with a drop of BacLight oil (Invitrogen), and covered with a glass slide (VWR, Cat. No. 631-0137). In the presented study, widefield epifluorescence microscopy (Zeiss, AxioCam-Imager M2) with a magnification of 100X equipped with Zeiss Zen<sup>lite</sup> software was employed for imaging. Each sample was imaged for 30 fields. The number of microbial cells per volume (cell/mL) would be counted and calculated following the equation (3):

$$B = \frac{N \times A_t}{d \times V_f \times G \times A_g} \quad (3)$$

where B is the number of microbial cells per volume (cell/mL), N is the total counted cells in the captured field, and A<sub>t</sub> represents the effective area of the filtered membrane, which equals 283.53 mm<sup>2</sup> in this study; d is denoted the dilution factor, while V<sub>f</sub> is the filtering volume of each sample, and G is the number of calculated captured fields in each sample. The area of the capturing view of the lens (A<sub>g</sub>) was assumed 0.01477 mm<sup>2</sup>. The average microbial cells per sample volume was calculated using Excel software.



#### 3.2.4.2 Enrichment of microbial communities from repository site groundwaters for pretesting and long-term experiments

Anaerobic culture media for the microbial enrichments was prepared targeting specific microbial groups such as e.g., sulfate reducing bacteria, iron cycling bacteria or manganese cycling microbes (Hallbeck & Pedersen 2008, Hegler et al., 2008). Shortly, the culture media components were mixed with milli-Q water in an Erlenmeyer bottle supplied with a magnet and boiled under constant stirring. Culture media was cooled on an ice bath under nitrogen purging, correct pH was verified and fixed if needed. Culture media was bottled for nitrogen purged headspace bottles or Schott bottles, equipped with butyl rubber stoppers and crimper rings, and further purged under nitrogen flow. The culture media was sterilized by autoclaving. Enrichment culture media was further supplied with additives when needed. The sampled groundwater was inoculated with a syringe technique into the enrichment culture media in an anaerobic glove box under a mixed gas atmosphere. The second inoculation into fresh culture media was done 4-6 weeks after the start of the incubation while also incubation of the first batch was continued. The enrichments were incubated at the +11°C temperature reflecting the in-situ conditions at repository depths.

#### 3.2.4.3 Experimental set-up for the pretesting of conditions

The effect of the LILW repository conditions on microbial communities evolves through time as the decreasing pH of the concrete pore water will no longer be able to suppress microbial activities or growth. To estimate how simulated evolved repository conditions, affect the microbial communities introduced by the repository groundwater, we will test the short-term effects of different simulated repository environments on microbes. In 2023, the anaerobic microbial enrichments of the repository site groundwaters (Loviisa and Olkiluoto) were started in May-June before the VTT microbiology laboratory moved to FutureHub2 facilities. In the autumn 2023, ATP-testing in anaerobic growth conditions and microbial enrichment cultures will be used together with the simulated groundwaters mimicking the evolved repository site. The preliminary tests cover the effect of pH on microbes with pH series with simulated concrete pore water. The measurement of ATP is used as a proxy for microbial metabolic activity. The ATP testing enables fast estimation of short exposure times on microbes and will be combined with other information on the microbial communities such as cell count enumeration (DAPI) as well as qPCR. In addition, pH and redox will be monitored.

#### 3.2.4.4 Metagenomic analysis of the former steel surface and water samples

Metagenomic samples originating from the repository site groundwater and from the TERKOR-project's long experiments (steel and water samples) were sequenced at Eurofins Genomics (<https://eurofinsgenomics.eu>). Metagenomic libraries were processed as 2 ×150 bp paired-end sequencing on the Illumina platform targeting to produce at least 10 million read-pairs for each sample. Metagenomic sequences were mainly analyzed and handled in the CSC Puhti supercomputer (<https://puhti.csc.fi>) under project 2008348. The quality of the raw sequences was first inspected with FASTQC (v. 0.11.9) for individual samples and merged into the quality report with the multiQC (v.1.15) program. The reads were checked, and paired-end Illumina reads merged with SeqPrep (v. 1.3.2), and low-quality sequences as well as Illumina-adaptor sequences were trimmed with Trimmomatic (v. 0.39) for both single and paired reads. Samples were co-assembled with MEGAHIT (v. 1.2.9) and assembly statistics were evaluated with Quast (v.5.2.0). Anvi'o contigs databases were built with Anvi'o (v. 7.1) for a minimum of 1500 bp long contigs with *anvi-gen-contigs-database* and merged to Anvi'o profile database with *anvi-merge*. Sequence reads were mapped back to the assembly with Bowtie2 (v.2.4.4) and samtools together with Anvi'o indexing. The metagenomic analysis will continue with automated binning with CONCONC and possible METABAT2 or MAXBIN2 followed by merging and optimization of the bins with DASTOOL2. After that, the bins will be manually curated in Anvi'o (v. 7.1). The final metagenome-assembled genomes (MAGs), as well as read-based sequence analysis, will be analysed for example for potential corrosion and biofilm formation related functional genes. Metagenomic analysis will continue 2023-2024. The next steps will also include building and testing new microbially influenced corrosion-related genetic databases and validation with current test data.

### 3.2.5 Water chemistry

All water chemistry samples were handled and analysed in ALS Global 5 days after sampling. Potentiometric titration methods were used for water pH, alkalinity and CO<sub>2</sub>. Spectrophotometric methods were used for phosphate, sulfides (H<sub>2</sub>S), ammonium (NH<sub>4</sub>), nitrite and nitrate analyses. Ionchromatographic methods were used for the analyses of sulfates and chlorides. Different metals were analyzed with ICP-MS, and Fe<sup>2+</sup> with UV-VIS method. IR-detector was used for the analyses of TOC and DOC.

## 4. Results

### 4.1 Electrochemical measurements

The potentiodynamic polarization curves of type 316L and 321 stainless steels (SS) measured at 22 °C in the simulated concrete pore water solution diluted with de-ionized water are shown in Figure 3. No significant differences are detected in the shape of the potentiodynamic curves for the different pH values, suggesting identical kinetics. There is a shift of the corrosion potential,  $E_{\text{corr}}$ , to more positive values as the pH decreases. This feature can be justified by the effect of pH on the cathodic process. Also, as pH increases more apparent passivation is visible in the anodic branch (Whitman et al., 1924). Passive current density reduces by more than one order of magnitude when pH is lowered from 14 to 7. While it is well accepted that the increase in the pH leads to the formation of thicker surface film (Olsson & Landolt, 2003), the reasons for the decrease of the passive current density were not explained. One of the next steps could be extending the potential window in the anodic direction or comparing the cyclic polarization curves to have a more complete view of the system. Alternatively, Freire et al. (2010) suggest that the lower current densities at lower pH are a consequence of the higher content of chromium on the surface via chromium oxides.

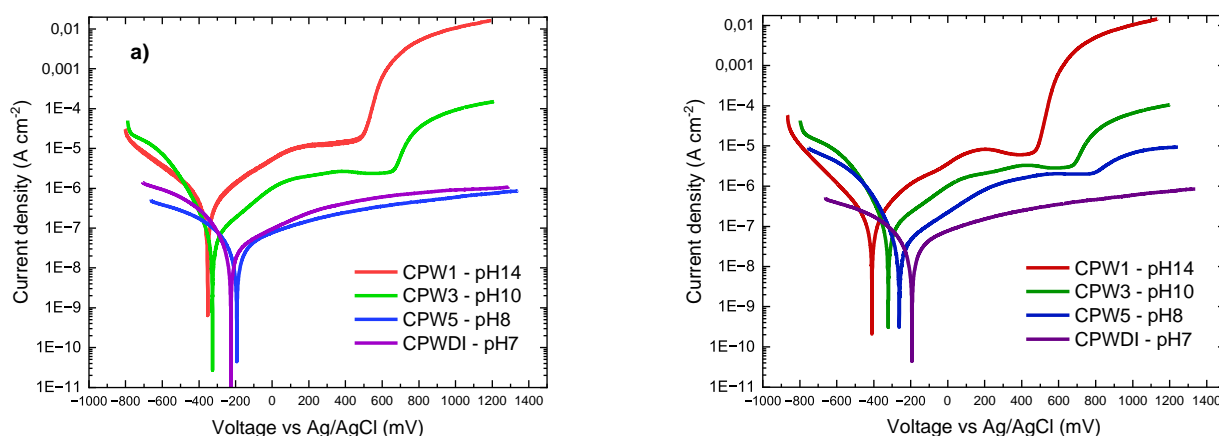


Figure 3. Potentiodynamic polarisation plots for a) 316L and b) 321 SS in the simulated concrete pore water solutions at different pH values (scan rate = 0,333 mV s<sup>-1</sup>).

Tests in the solutions of simulated groundwater type 316 and 321 SS showed a typical anodic polarization behaviour of stainless steel in the presence of chlorides consisting of active dissolution, passivity, and a rapid increase in the current density due to pitting (Figure 4). This rapid increase in the current density indicates the occurrence of the stable pitting in which the potential corresponding to this current transient is known as a critical pitting potential,  $E_{\text{pit}}$  (Jones, 1996). Other common characteristic shapes of the potentiodynamic polarization curves were observed. However, significant differences can be noted in the

corrosion potential ( $E_{\text{corr}}$ ), corrosion current density ( $i_{\text{corr}}$ ), and passive current density ( $i_{\text{pass}}$ ) across pH and solutions. Similar to the tests performed in the simulated concrete pore water, there is a shift to more positive corrosion potentials as pH decreases. Interestingly,  $i_{\text{pass}}$  of 316L (Figure 4a) is the biggest for the curves measured in CPW with pH 14, the lowest – in CPW with pH 8 and 7, and the intermediate values are attributed to stainless steels measured in groundwater. 321 stainless steel (Figure 4b) while also showing the highest  $i_{\text{pass}}$  values for CPW pH 14 solution, the next biggest values are exhibited by curves measured in groundwaters. Also, compared to the samples in GW, the CPW curve in Figure 4 did not show a clear indication of the stable pitting until the transpassive potential region. This transpassive dissolution of type 316L SS is due to the oxidative dissolution of Cr oxide, which is observed in solutions with no chloride ions (Fattah-alhosseini et al., 2009).

In Figure 4b some current density spikes are observed at potentials below  $E_{\text{pit}}$ . These spikes are due to the occurrence of metastable pits and are explained by the consecutive formation and repassivation of microsize pits (Zhang et al., 2012). Comparing curves together, the frequency and magnitudes of the spikes appear to be most apparent for 321 SS in pure simulated groundwater. Figure 5 summarizes all the curves measured for 316L (Fig. 5a) and 321 (Fig. 5b) in various solutions.

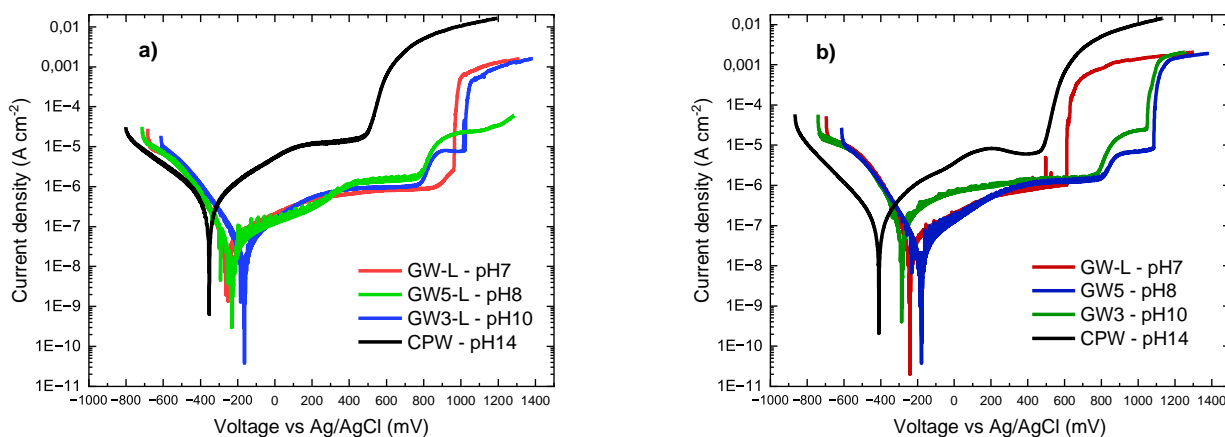


Figure 4. Potentiodynamic polarisation plots for a) 316L and b) 321 SS in the simulated concrete pore water (CPW) solutions and groundwater (GW) solutions mixed with CPW at different pH values (scan rate = 0,333 mV s<sup>-1</sup>).

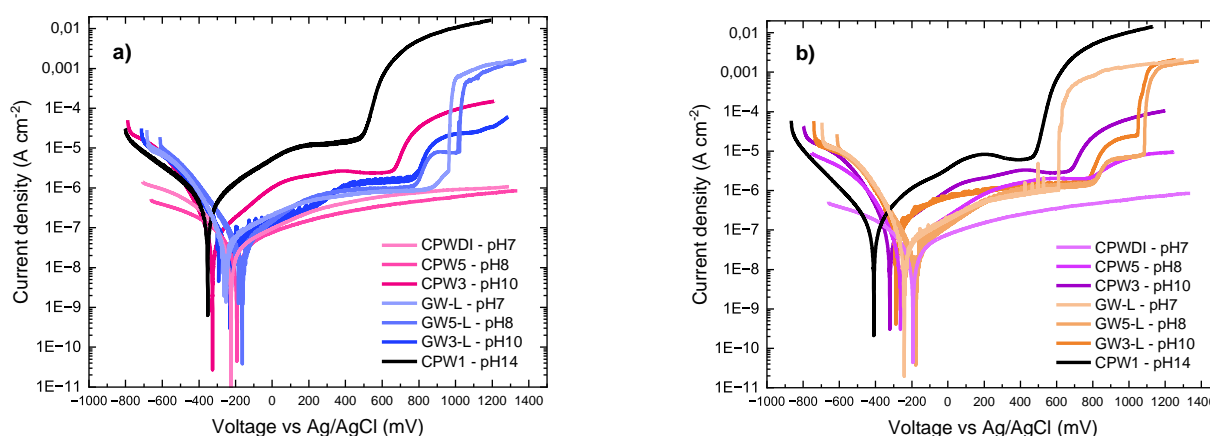


Figure 5. A summary of potentiodynamic polarisation plots for a) 316L and b) 321 SS in the simulated concrete pore water (CPW) solutions and groundwater (GW) solutions mixed with CPW at different pH values (scan rate = 0,333 mV s<sup>-1</sup>).

The values of all the potential points,  $E_{corr}$ ,  $E_{pp}$ ,  $E_{p1}$  (corrosion, primary passivation, transpassive, and pitting potentials) determined from the polarization curves are listed in Table 4. As mentioned, corrosion potentials tend towards more positive values with the pH decrease. For some curves it is difficult to detect the primary passivation potential, so wider potential window can be used for further measurements. The most striking difference is overall higher pitting potential of the 316L steel, especially in pure groundwater at pH 7. The high pitting resistance of the 316L SS can be attributed to the presence of nitrogen as an alloying element and it can easily form a highly stable phase of iron nitride FeN. This can increase the inhibition of the pit formation and it increases the chances for pit the healing process (Dhaiveegan et al., 2016).

Table 4. Corrosion, passivation, pitting, and corrosion rate values of the materials (316L/321) tested in the concrete pore water and ground water solutions at different pH.

316L / 321	$E_{corr}$ (mV vs Ag/AgCl)	$E_{pp}$ (mV vs Ag/AgCl)	$E_{p1}$ (mV vs Ag/AgCl)	Corrosion rate (*10 <sup>-3</sup> mm per year)
CPW - pH14	-352 / -409	200 / 206	495 / 476	13.06 / 5.173
CPW3 - pH10	-326 / -321	381 / 430	659 / 675	2.204 / 3.000
CPW5 - pH8	-193 / -261	x* / 570	x / x	1.250 / 1.044
CPWDI - pH7	-225 / -193	x / x	x / x	1.240 / 1.295
GW3-L - pH10	-231 / -286	x / x	781 / 770	0.487 / 5.141
GW5-L - pH8	-163 / -178	x / x	781 / 812	0.9755 / 0.7678
GW-L - pH7	-251 / -240	x / x	960 / 610	1.448 / 1.147

\*x – no information obtained from the curve

## 4.2 Surface analysis

Figure 6 presents the microscopy images of the two kinds of steel 316L and 321 after potentiodynamic measurements in simulated concrete pore water solutions. No visible pits appear on the surface of these steels, however some smaller pits and surface irregularities may be visible under other microscopic techniques (e.g., scanning electron microscopy).

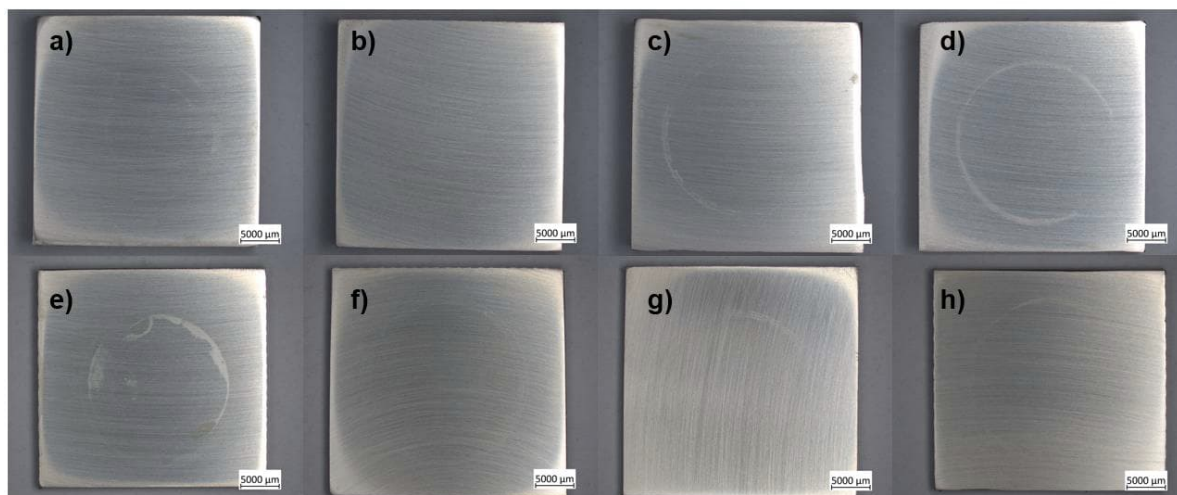


Figure 6. Microscopy images of the a-d) 316L and e-h) 321 stainless steel after potentiodynamic polarization measurements ( $-500\text{ mV} / + 1500\text{ mV}$  vs  $E_{ocp}$ ,  $0.333\text{ mV/s}$ ) in simulated concrete pore water: a, e) pH 14, b, f) pH 10, c, g) pH 8, d, h) pH 7.

By contrast, pits appear in the steel coupons after polarization measurements in the simulated groundwater (Figure 7). Notably, the amount of the pits appears to increase with the decrease in pH. Also, 316L seems to be more resistant to the simulated GW compared to the 321, as the latter exhibits intensive pits at pH 10 (Figure 7d) while there is none visible in the former at pH 10.

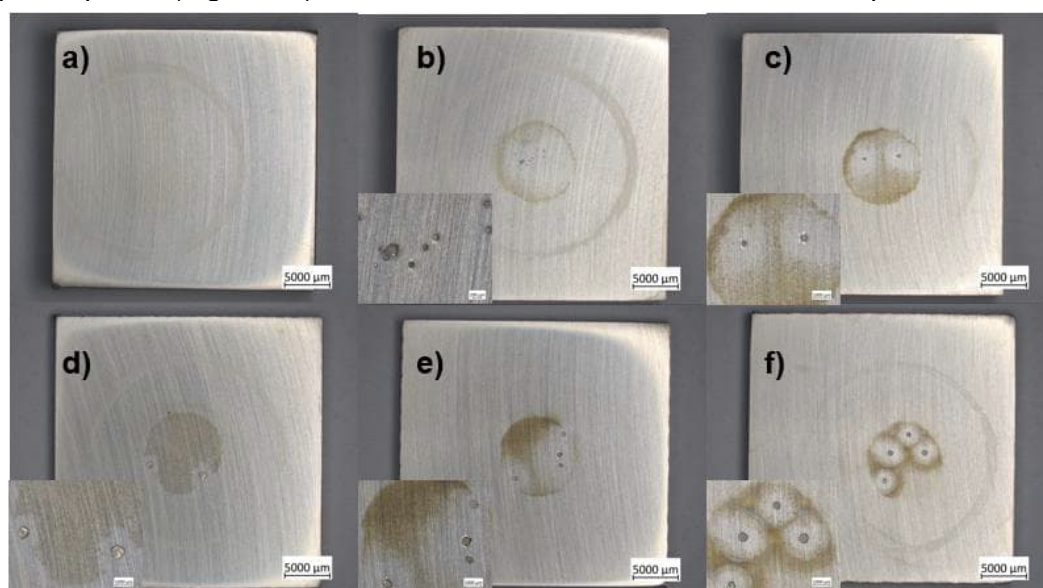


Figure 7. Microscopy images of the a-c) 316L and d-f) 321 stainless steel after potentiodynamic polarization measurements ( $-500\text{ mV} / + 1500\text{ mV}$  vs  $E_{ocp}$ ,  $0.333\text{ mV/s}$ ) in simulated groundwater: a, d) pH 10, b, e) pH 8, c, f) pH 7. The insets represent the magnified region of pitting (in case there is pitting).

### 4.3 Water chemistry simulations

In order to improve the understanding of the principles of the interaction of groundwater with cured cement that contains concrete porewater, basic thermodynamic calculations were performed using the Equilibration Module of the Metso:Outotec HSC Chemistry 10 software in version 10.3.7.1. The goal was

to understand the development of the pH value and the chloride concentration in the groundwater as these two parameters are important for the corrosion behavior of the studied metals.

For the simulations, a fictive case was assumed, in which simplified cured cement consisting of calcium silicate hydrate ( $3 \text{ CaO} \cdot 2 \text{ SiO}_2 \cdot 3 \text{ H}_2\text{O}$ ), portlandite ( $\text{Ca}(\text{OH})_2$ ) and ettringite ( $3 \text{ CaO} \cdot \text{Al}_2\text{O}_3 \cdot 3 \text{ CaSO}_4 \cdot 32 \text{ H}_2\text{O}$ ) that contained simplified concrete porewater containing sodium hydroxide, potassium hydroxide and potassium sulphate was diluted successively with simplified groundwater. The composition of the simplified porewater was based on the chemical analyses done by Lothenbach et al. (2008). The chemical components of the simplified groundwater were chosen so that they resemble the water type from borehole HH-KR1 in depths T6 and T7 as analyzed in 2004 (Hatanpää, 2006).

The initial amount of cured cement in the simulation was about 1.7 kg containing about 1 kg concrete porewater to which about 10000 kg groundwater were successively added so that the dilution of the porewater was 10000 times. It was assumed that the components of the cured cement as well as the solid substances, which were allowed to form, consisted of pure substances that don't interact with each other. Consequently, their activity coefficient was set to 1 in the calculations. For the water phase, the 'aqua' solution model of the HSC 10 Equilibration Module was used to perform the calculations not simply with the concentrations of the assumed chemical species but with their activities according to Pitzer. A temperature of 25 °C was assumed. Two slightly different simulations were calculated. The first run did not allow the formation of Ca and Mg silicates, like serpentine, which were included in the second run. Table 5, Table 6 and Table 7 give an overview on the used chemical species and their amounts in the simulations.

*Table 5. Overview on the chemical species included in the simplified thermodynamic simulation. All substances listed here were treated as single phases having an activity coefficient of 1.*

Chemical formula	HSC 10 notation	Initial mol	Initial kg	Final mol	Final kg
Concrete			1.672		
$3 \text{ CaO} \cdot 2 \text{ SiO}_2 \cdot 3 \text{ H}_2\text{O}$	*3CaO*2SiO2 *3H2O	1.000	0.342		
$3 \text{ CaO} \cdot \text{Al}_2\text{O}_3 \cdot 3 \text{ CaSO}_4 \cdot 32 \text{ H}_2\text{O}$	Ca6Al2(SO4)3(OH)12*26H2O	1.000	1.255		
$\text{Ca}(\text{OH})_2$	Ca(OH)2	1.000	0.074		
Porewater			1.053		
$\text{H}_2\text{O}$	H2O	55.508	1.000		
NaOH	NaOH	0.400	0.016		
KOH	KOH	0.570	0.032		
$\text{K}_2\text{SO}_4$	K2SO4	0.030	0.005		
Groundwater			0.000		10084.083
$\text{H}_2\text{O}$	H2O	0.000	0.000	555084.351	10000.000
NaCl	NaCl	0.000	0.000	710.000	41.494
$\text{CaCl}_2$	CaCl2	0.000	0.000	220.000	24.416
$\text{MgCl}_2$	MgCl2	0.000	0.000	110.000	10.473
$\text{MgSO}_4$	MgSO4	0.000	0.000	50.000	6.018
$\text{NaHCO}_3$	NaHCO3	0.000	0.000	20.000	1.680



Table 6. List of soluble species that were allowed to form during the thermodynamic simulation. The 'aqua' solution model of the HSC 10 software was used considering also the activities of the ions according to Pitzer.

Chemical formula	HSC 10 notation	Chemical formula	HSC 10 notation	Chemical formula	HSC 10 notation
Water					
H <sub>2</sub> O	H2O	H <sup>+</sup>	H(+a)	OH <sup>-</sup>	OH(-a)
Na <sup>+</sup>	Na(+a)	NaOH · aq	NaOH(a)	K <sup>+</sup>	K(+a)
KOH · aq	KOH(a)	Mg <sup>2+</sup>	Mg(+2a)	MgOH <sup>+</sup>	Mg(OH)(+a)
MgCl <sup>+</sup>	MgCl(+a)	Ca <sup>2+</sup>	Ca(+2a)	CaOH <sup>-</sup>	CaOH(-a)
CaCl <sup>-</sup>	CaCl(-a)	Al <sup>3+</sup>	Al(+3a)	AlOH <sup>2+</sup>	AlOH(+2a)
Al(OH) <sub>2</sub> <sup>+</sup>	Al(OH)2(+a)	Al(OH) <sub>3</sub> · aq	Al(OH)3(a)	Al(OH) <sub>4</sub> <sup>-</sup>	Al(OH)4(-a)
AlCl <sub>3</sub> · aq	AlCl3(a)	SiO <sub>4</sub> <sup>4-</sup>	SiO4(-4a)	SiO <sub>3</sub> (OH) <sup>3-</sup>	SiO3(OH)(-3a)
SiO <sub>2</sub> (OH) <sub>2</sub> <sup>2-</sup>	SiO2(OH)2(-2a)	SiO(OH) <sub>3</sub> <sup>-</sup>	SiO(OH)3(-a)	HSiO <sub>3</sub> <sup>-</sup>	HSiO3(-a)
CO <sub>3</sub> <sup>2-</sup>	CO3(-2a)	HCO <sub>3</sub> <sup>-</sup>	HCO3(-a)	SO <sub>4</sub> <sup>2-</sup>	SO4(-2a)
HSO <sub>4</sub> <sup>-</sup>	HSO4(-a)	Cl <sup>-</sup>	Cl(-a)		

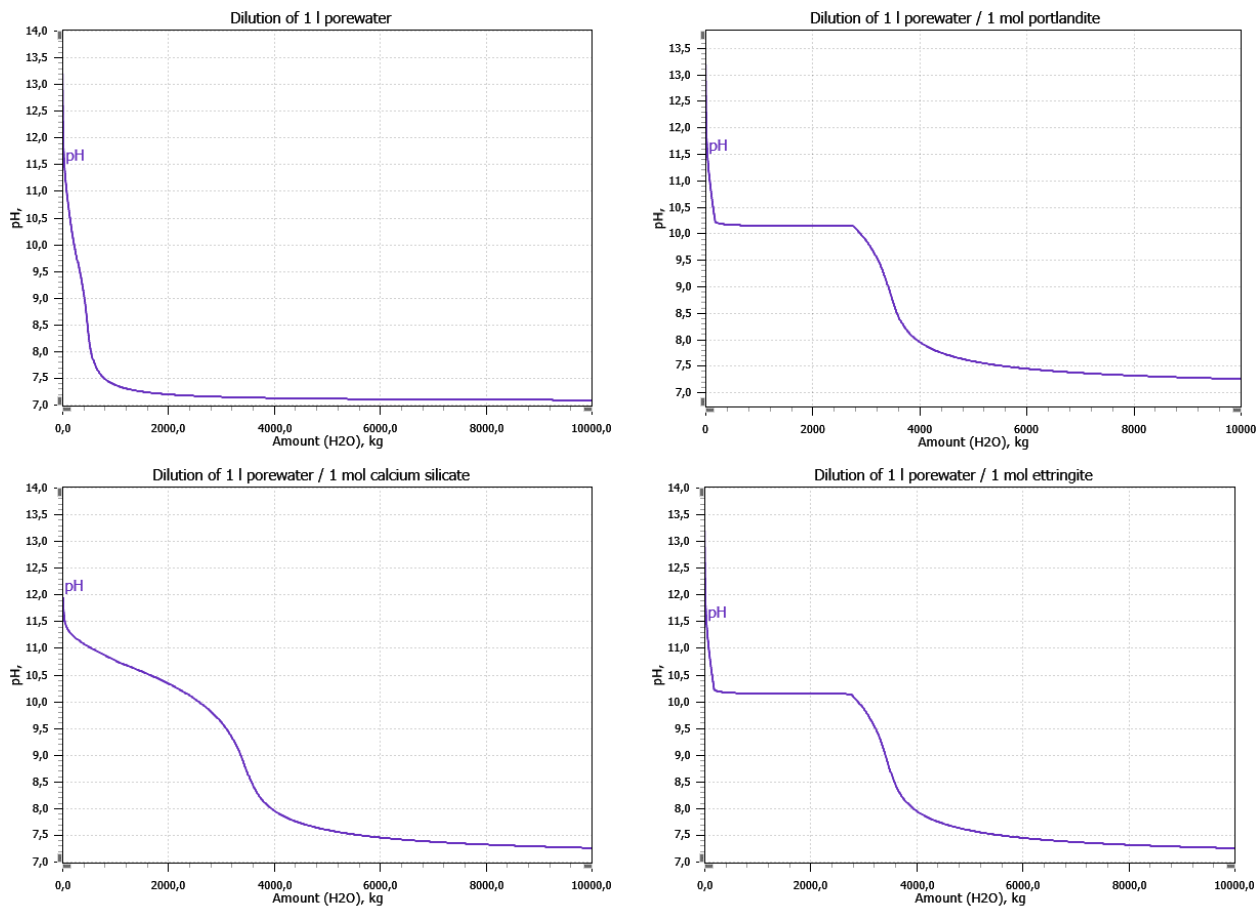
Table 7. List of solid substances that were allowed to form during the thermodynamic simulation. All substances listed here were treated as single phases having an activity coefficient of 1. The additional solids were included only in the second simulation.

Chemical formula	HSC 10 notation	Name	Chemical formula	HSC 10 notation	Name
Deposits					
Al(OH) <sub>3</sub>	Al(OH)3	Aluminum hydroxide	Al <sub>2</sub> O <sub>3</sub>	Al2O3	Aluminum oxide
H <sub>2</sub> SiO <sub>3</sub>	H2SiO3	Metasilicic acid	H <sub>4</sub> SiO <sub>4</sub>	H4SiO4	Orthosilicic acid
SiO <sub>2</sub>	SiO2	Silicon dioxide	NaAlSi <sub>3</sub> O <sub>8</sub>	NaAlSi3O8	Albite
KAlSi <sub>3</sub> O <sub>8</sub>	KAlSi3O8	Orthoclase	CaSO <sub>4</sub>	CaSO4	Anhydrite
CaSO <sub>4</sub> · ½ H <sub>2</sub> O	CaSO4*0.5H2O	Plaster of Paris	CaSO <sub>4</sub> · 2 H <sub>2</sub> O	CaSO4*2H2O	Gypsum
CaCO <sub>3</sub>	CaCO3	Limestone			
Additional deposits					
MgSiO <sub>3</sub>	MgSiO3	Magnesium metasilicate	Mg <sub>2</sub> SiO <sub>4</sub>	Mg2SiO4	Magnesium orthosilicate
CaSiO <sub>3</sub>	CaSiO3	Calcium metasilicate	Ca <sub>2</sub> SiO <sub>4</sub>	Ca2SiO4	Calcium orthosilicate
3 MgO · 2 SiO <sub>2</sub> · 2 H <sub>2</sub> O	*3MgO*2SiO2*2H2O	Serpentine	3 MgO · 4 SiO <sub>2</sub> · H <sub>2</sub> O	*3MgO*4SiO2*H2O	Talc



### 4.3.1 Simulation excluding the formation of magnesium and calcium silicates

The effect of the presence of the three different cured cement components on the evolution of the pH value is illustrated in Figure 8. When only alkaline porewater without cement is diluted with neutral groundwater, the pH value drops relatively fast to neutral values due to the dilution of the porewater. When 1 mol portlandite is assumed to be present in contact with the porewater, the additional  $\text{Ca}(\text{OH})_2$  in the system needs to be neutralized, too. Consequently, the pH value drops after more groundwater has been added than in the case before. When 1 mol calcium silicate is added to the porewater that is diluted, the pH value is initially lower, but reaches neutral values even more groundwater additions. When 1 mol ettringite is put into the calculations besides the porewater, a pH buffer forms at pH value 10.1, which needs to be diluted before the pH finally can drop to the level of the groundwater. When all three main constituents of cured cement are included in the simulation, the pH value drops after only a few dilution cycles significantly as also observed before. It then remains at values over 10 despite continuous dilution with groundwater until it drops to 8.8 where a second, new and shorter pH buffer range exists. When this buffer is finally diluted sufficiently, the pH reaches slowly the neutral values of the groundwater.



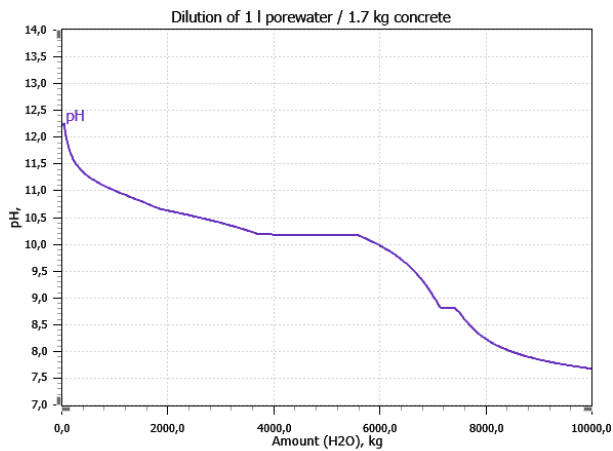


Figure 8. Calculated pH values during the dilution of porewater containing different solid main components of concrete. See the headings of the plots for details.

When looking at the anions in the aqueous phase (see Figure 9), the reasons for the different steps in the pH curve during the dilution of the porewater and concrete with groundwaters become clear. The initial slowdown in the pH curve is related to the formation of silicate buffers. The following larger plateau at pH value 10.1 is caused by an aluminate buffer. The last short plateau at pH 8.8 is the manifestation of a carbonate buffer system that is caused by hydrogen carbonate in the groundwater.

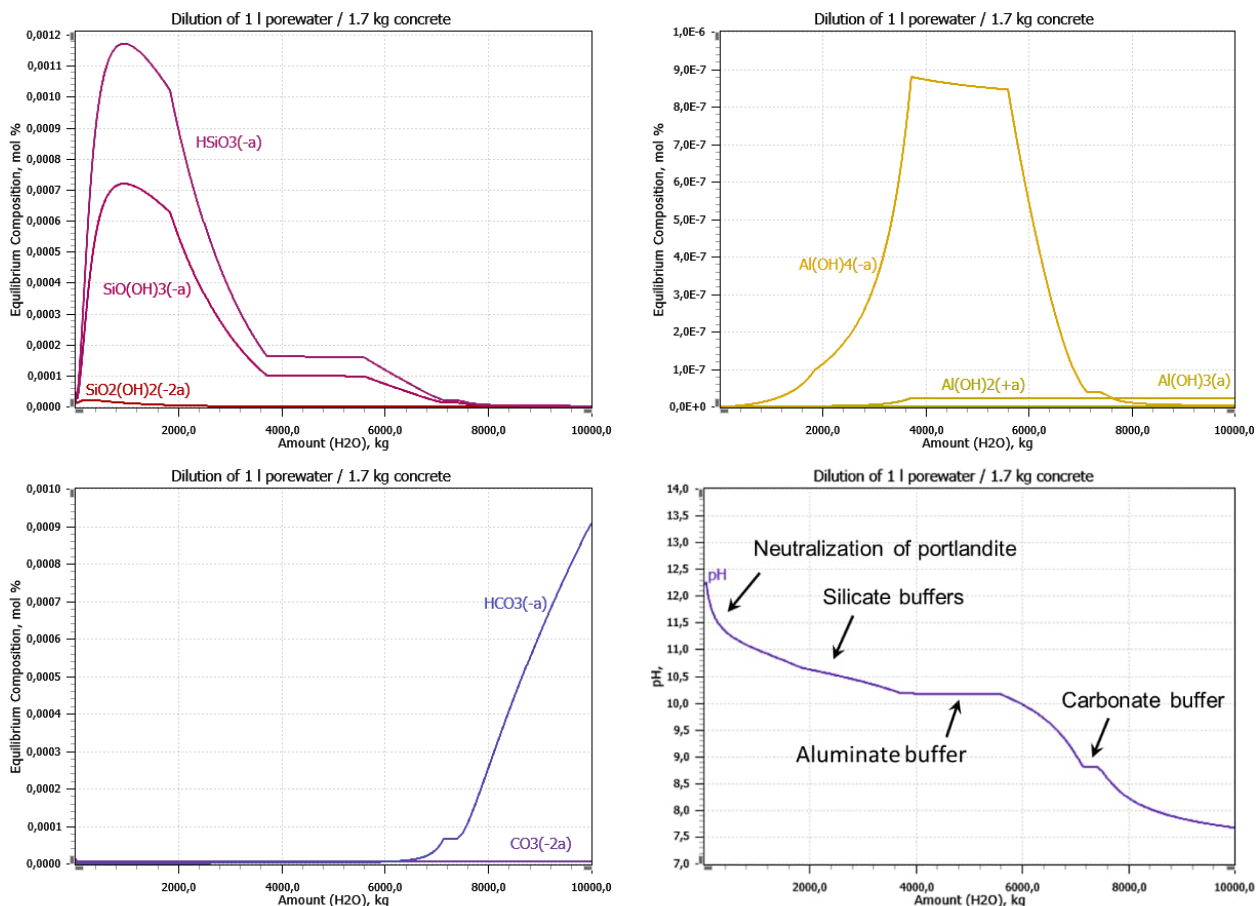


Figure 9. Calculated amounts of the major silicon (upper left plot), aluminum (upper right plot) and carbon (lower left plot) containing compounds in the aqueous phase and their relation to the pH curve (lower right plot).

As can be seen from Figure 10, the model predicts that the cured cement should start to dissolve after relatively small additions of groundwater due to the dissolution of portlandite. Also, the selected calcium silicate form is not stable in this simulation. When the cured cement is dissolved in the added groundwater, deposits can form from the species in the groundwater and the compounds that originate from the dissolved cement. The main component that is deposited is limestone but also aluminum oxide and silicic acid form finally. Intermediately, also albite and orthoclase occur. It should be noticed that no calcium sulphates are depositing according to the calculations, not even intermediately.

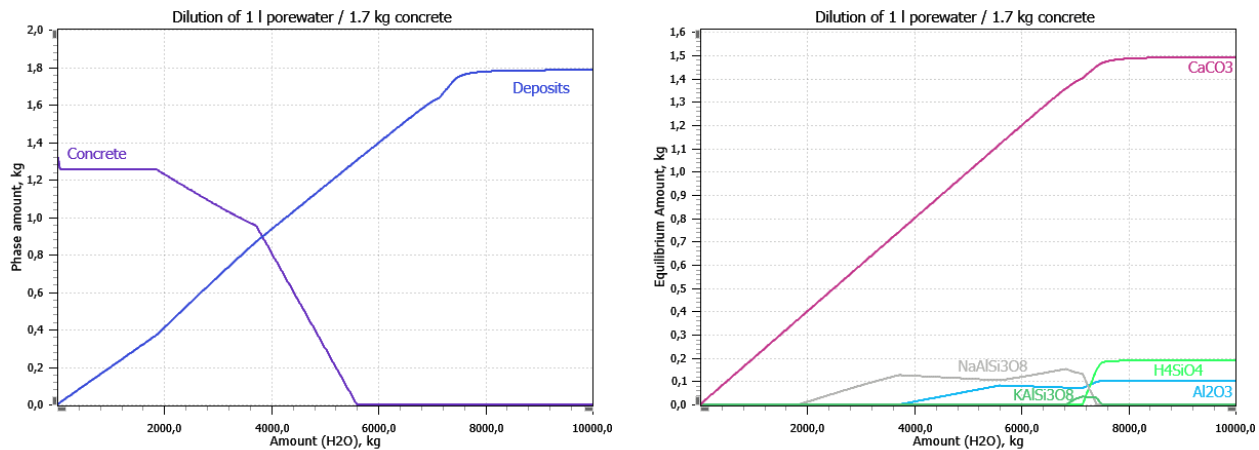


Figure 10. Amount of concrete and deposits during the dilution of concrete porewater with groundwater (left plot) as well as the more detailed composition of the formed deposits (right plot).

As can be seen from Figure 11, the chloride concentration stabilizes after relatively small amounts of groundwater, compared to the whole amount of groundwater used in the simulation, are added to the concrete porewater. When the porewater is diluted by about 100 times, the chloride content reaches roughly the chloride level of the groundwater. Chloride occurs in the simulation mainly chloride ions. Only very small amounts of magnesium and calcium chloride complexes may be encountered.

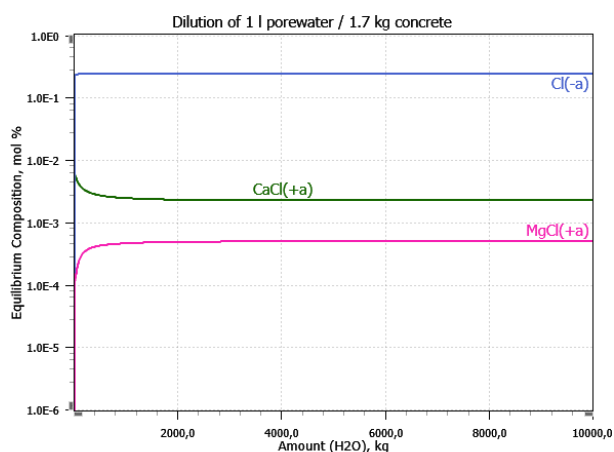


Figure 11. Calculated concentration of chloride and chloride complexes during the dilution of porewater containing different main components of concrete.

#### 4.3.2 Simulation including the formation of magnesium and calcium silicates

Assuming that magnesium and calcium silicates, like serpentine, may also deposit during the dilution of concrete porewater with groundwater in the presence of cured concrete, the thermodynamic simulation

indicates that the pH value of the resulting aqueous solution drops after relatively small additions of groundwater. After the first pH decrease, two pH buffer ranges are observed (see Figure 12) that are separated by a second steeper decrease in the pH value. The silicate buffer occurring after low groundwater additions, which was observed in the simulation presented before, is no longer active. The aluminate buffer at pH 10.1, however, is still observed. The carbonate buffer range, which was observed after the cured cement had dissolved in the groundwater, is clearly larger when magnesium and calcium silicates are considered in the simulation. As the pH value of the buffer is 7.9, which is relatively low for a carbonate buffer, it could be assumed that carbonate might interact with silicates creating a buffer that has a lower pH value than 8.8 which was observed in the simulation excluding the formation of serpentine.

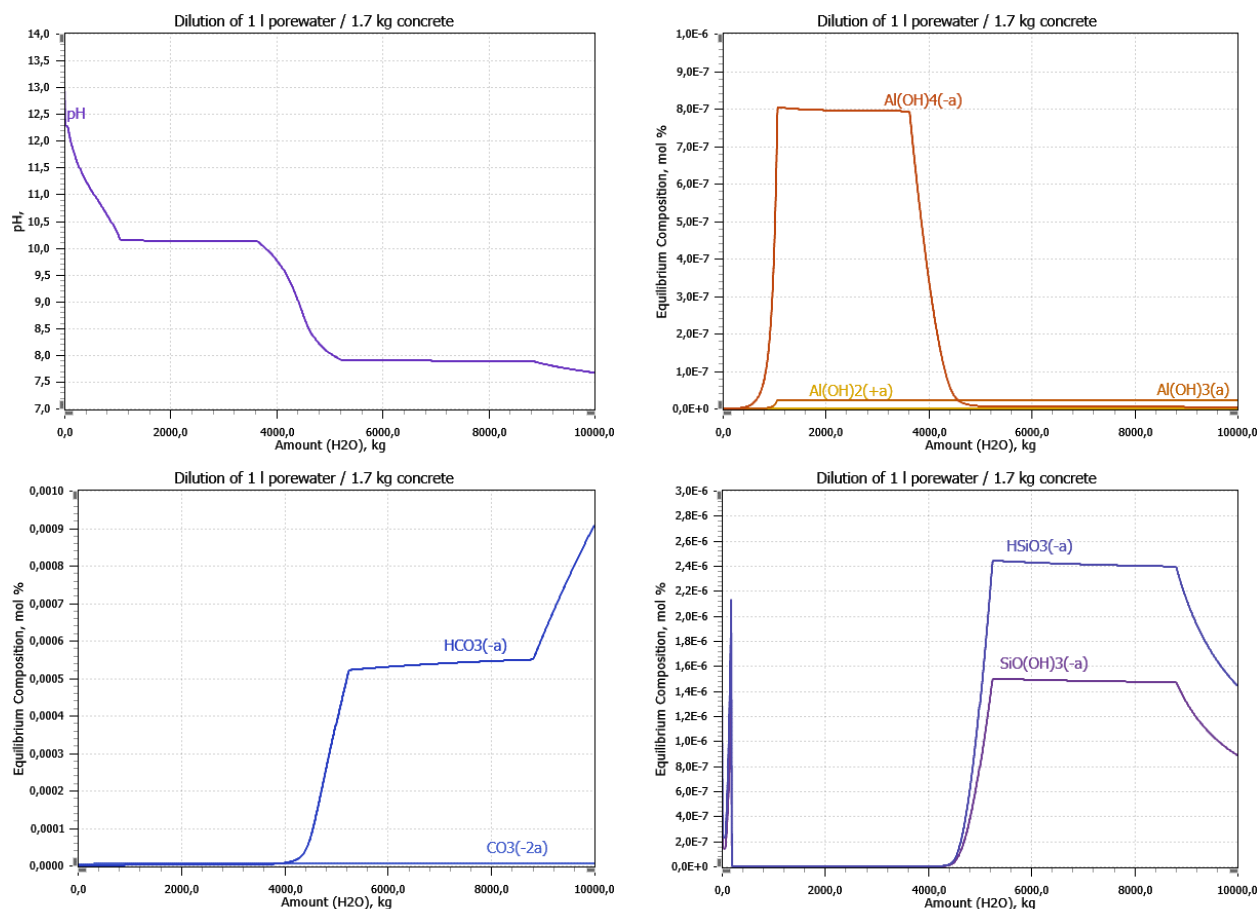


Figure 12. Calculated pH value of concrete porewater as function of the added groundwater amount (upper left plot) and corresponding concentrations of aluminum (upper right plot) compounds as well as of carbonate (lower left plot) and silicate (lower right plot) species forming the buffer ranges occurring in the pH curve.

As can be seen from Figure 13, concrete may dissolve in a smaller amount of water when serpentine is allowed to form. At the same time, the occurrence of albite and orthoclase is no longer favorable.

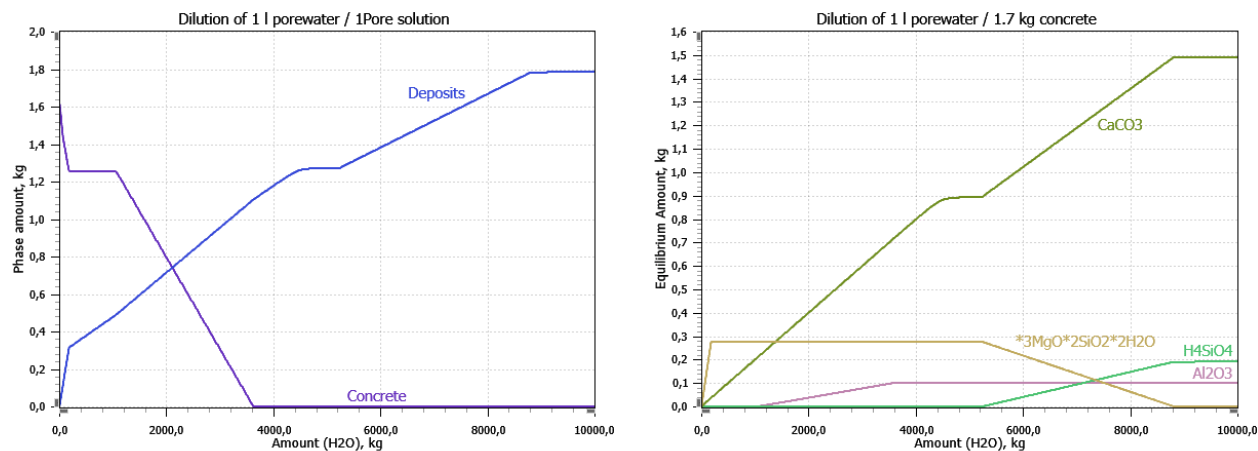


Figure 13. Amount of concrete and deposits during the dilution of concrete porewater with groundwater (left plot) as well as the more detailed composition of the formed deposits (right plot). Less groundwater is needed to cause the dissolution of the concrete phase when serpentine is allowed to form in the simulation.

#### 4.3.3 Validity of the thermodynamic simulation results

Thermodynamic calculations as presented above are commonly affected by the selected parameters on which the simulation is based and on the quality of the underlying thermodynamic data. The used software is not specialized in concrete so probably not all species that may be encountered in ageing concrete were considered. Also, the boundaries under which the simulation is performed influence its outcome. Some examples are presented in Figure 14. When it is, for instance, assumed that the deposits that form during the interaction of the groundwater with the concrete and porewater are not pure solids but form all one ideal mixture, the sections of the resulting pH curve are not that clearly separated, and the pH level is generally somewhat higher. When another calcium silicate variant is chosen for the simplified concrete from the database of the simulation software, it may have a lower solubility in the groundwater resulting in a slightly different pH curve.

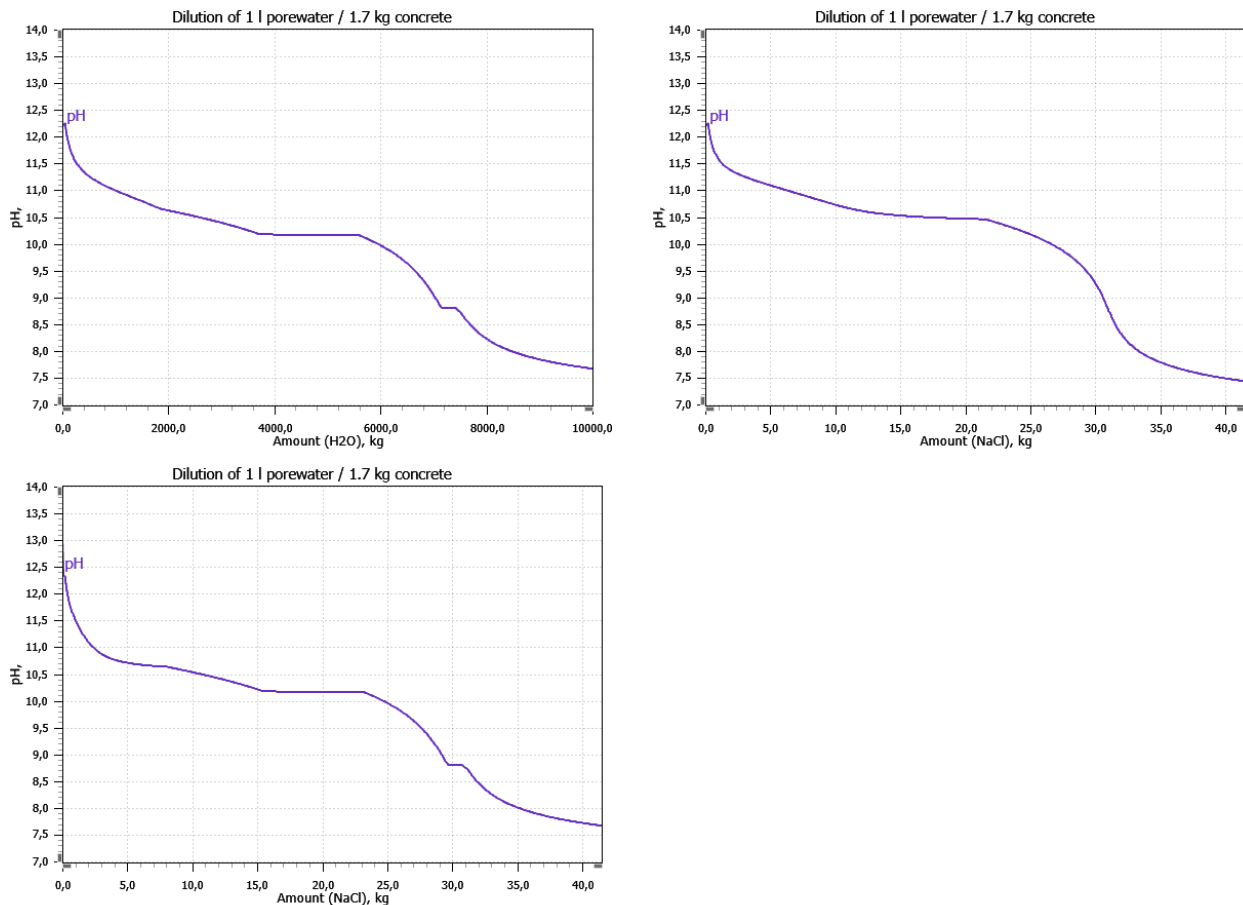


Figure 14. Calculated pH values during the dilution of porewater containing different solid main components of concrete. The left plots were calculated under the assumption that the different deposits that form during the contact of the groundwater with the concrete and porewater are pure solids that don't mix with each other. In the right plot, it was assumed that the different deposits form an ideal mixture. The difference between the left upper and lower plots is that different calcium silicates were chosen. The variant in the upper plot dissolved complete already in a relatively small amount of ground water.

Additionally, it has to be considered that the presented results of the thermodynamic simulations are based on assumptions that most probably don't manifest themselves in the field exactly as expected. Especially the quantitative relations between concrete, porewater and groundwater were chosen with the intent to identify and understand the factors that influence the water chemistry of concrete and porewater during the exposure to groundwater at the repository sites which are important for the corrosion processes of the studied metals. In practice, these relations may be very different to what was used for the presented calculations. Additionally, it has to be considered that the thermodynamic calculations are done with the assumption that an equilibrium is reached immediately at each calculated data point. This is surely not true in the real world because the occurring dissolution and deposition processes are perhaps governed but at least influenced by reaction kinetics and diffusion processes in the concrete environment, which are not considered in the presented calculation results.

The presented thermodynamic calculations indicate that different silicate, aluminate and carbonate buffers may be observed during the dilution of concrete porewater with groundwater which may fix the pH value of the concrete porewater/groundwater mixtures during the evolution of repository for some time on different levels. This means that more groundwater than one would normally expect will be needed to neutralize the porewater in the concrete. The results indicate also that the concrete needs to be dissolved completely before the pH value can drop to neutral values because it acts as a source for species that

increase the pH value of the groundwater. Another result of the simulations that is important for the corrosion behaviour of the tested metals is that the chloride content in the diluted porewater adjusts after about 100 dilutions of the porewater with groundwater to the values found in the groundwater. Additionally, the calculations reveal that limestone will probably form from the dissolving concrete and the bicarbonate in the groundwater. This is important for the corrosion of carbon steel because limestone deposits are known to protect carbon steel from corrosion in neutral natural waters, like the also formed dissolved silicates.

#### 4.4 Enumeration of microbial cell counts in repository site waters

DAPI-staining and calculation reveal the difference between the average microbial cell number presenting in water samples collected in Loviisa and Olkiluoto. For instance, approximately **147 490 ± 871 cells/mL** were detected in repositorial groundwater in Loviisa, while about **434 467 ± 962 cells/mL** were detected in water sample collected in Olkiluoto. Based on the estimation, it suggests that the microbial abundance in water in Olkiluoto was about 3 times higher than in Loviisa. Figure 15 and Figure 16 represent DAPI-stained images of water samples collected in two locations using epifluorescence microscopy.

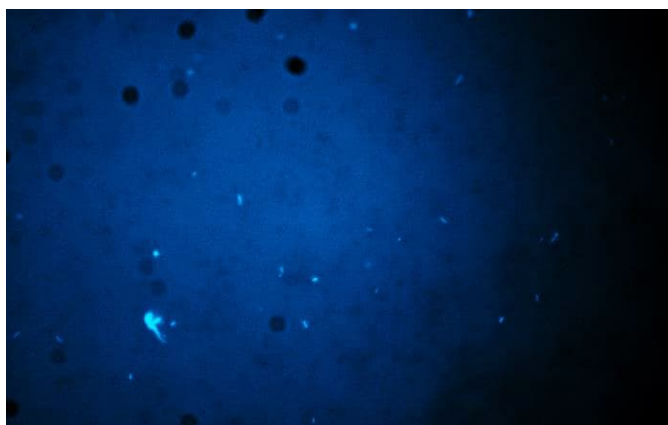


*Figure 15. Representative image of DAPI stained microbial cells in collected water sample in Loviisa in May 2023.*

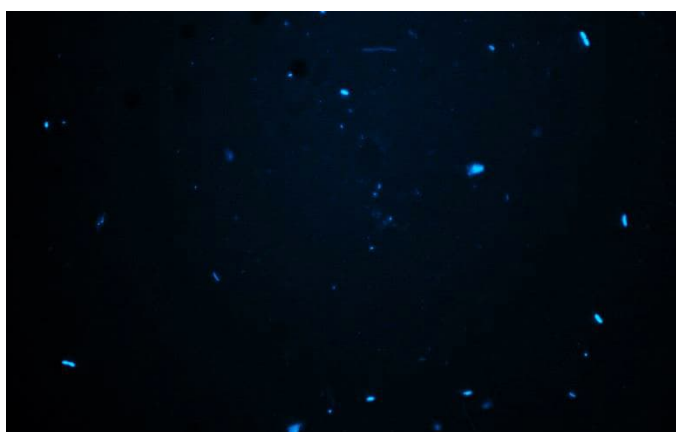


*Figure 16. Representative image of DAPI stained microbial cells in collected water sample in Olkiluoto in June 2023.*

#### 4.5 Water chemistry of the repository site groundwaters

Repository site water chemistries differed from each other as also previously reported (Somervuori et al., 2021). The pH in Loviisa was 7.7 and in Olkiluoto a little higher 8.4 (Table 8). Olkiluoto groundwater hosted higher levels of dissolved organic carbon (DOC,  $7.19 \pm 1.44$  mg/L) and total organic carbon (TOC,  $7.8 \pm$



1.56 mg/L), whereas Loviisa groundwater had higher chloride concentrations (4980 mg/L) than Olkiluoto groundwater (623 mg/L).

Loviisa waters contained higher levels of sulfate ( $576 \pm 86.4$  mg/L) compared to sulfate levels in Olkiluoto ( $157 \pm 23.6$  mg/L). However, sometimes sulfate levels in groundwater may fluctuate for example due to microbial activities. Phosphate levels were higher in Olkiluoto groundwater ( $0.167 \pm 0.033$  mg/L) and remained under detection limit in Loviisa.

*Table 8. Water chemistries at repository site groundwaters in Loviisa and Olkiluoto. Please see Appendix for full analysis report and limitations.*

Analysis	Unit	Loviisa	Olkiluoto
pH		$7.73 \pm 0.08$	$8.38 \pm 0.08$
DOC	mg/L	$0.96 \pm 0.19$	$7.19 \pm 1.44$
TOC	mg/L	$1.95 \pm 0.39$	$7.8 \pm 1.56$
Alkalinity, pH 4.5	mmol/L	$1.76 \pm 0.211$	$5.26 \pm 0.632$
Alkalinity, pH 8.3	mmol/L	<0.150	<0.150
Chlorides	mg/L	$4980 \pm 746$	$623 \pm 93.4$
Carbonates (CO <sub>3</sub> <sup>2-</sup> )	mg/L	0.0	$3.65 \pm 0.44$
Acidity pH 8.3	mmol/L	$0.157 \pm 0.024$	<0.150
Acidity, pH 4.5	mmol/L	<0.150	<0.150
HCO <sub>3</sub> <sup>-</sup>	mg/L	$107 \pm 12.9$	$314 \pm 37.7$
Carbon dioxide, total	mg/L	$84.4 \pm 10.1$	$229 \pm 27.5$
Carbon dioxide, free	mg/L	$6.91 \pm 0.83$	0.0
Aggressive carbon dioxide	mg/L	$4.80 \pm 0.58$	0.0
Sulfide (H <sub>2</sub> S)	mg/L	< 0.05	< 0.05
Sulfide (S <sup>-</sup> )	mg/L	< 0.05	< 0.05
Sulfate	mg/L	$576 \pm 86.4$	$157 \pm 23.6$
Ammonium	mg/L	$0.794 \pm 0.119$	$0.24 \pm 0.036$
Ammonium nitrogen	mg/L	$0.617 \pm 0.092$	$0.186 \pm 0.028$
Nitrite	mg/L	<0.005	<0.005
Nitrite nitrogen	mg/L	<0.002	<0.002
Nitrate	mg/L	<0.66	<0.27
Nitrate nitrogen	mg/L	<0.150	<0.06
Phosphate	mg/L	<0.04	$0.167 \pm 0.033$
Phosphate phosphorus	mg/L	<0.013	$0.054 \pm 0.011$
Si	mg/L	$4.83 \pm 0.5$	$6.72 \pm 0.7$
S	mg/L	$190 \pm 19$	$51.5 \pm 5.1$
Fe <sup>2+</sup>	mg/L	$0.017 \pm 0.007$	$0.055 \pm 0.009$

There were also differences in the levels of analysed soluble metals in repository site groundwaters. The levels of soluble calcium, magnesium, manganese, potassium and sodium were higher in Loviisa site waters, whereas Olkiluoto groundwater had higher levels of iron (Table 9).



Table 9. Soluble metals in water samples in Loviisa and Olkiluoto in 2023. Please see Appendix for full analysis report and limitations.

Soluble metals	Unit	Loviisa	Olkiluoto
Hg	µg/L	<0.005	<0.0050
Al	µg/L	<20.0	5.8 ± 0.6
Ba	µg/L	31.5 ± 3.15	19.1 ± 1.91
Be	µg/L	<1.00	<0.20
B	µg/L	339 ± 34	445 ± 44
Ca	µg/L	671000 ± 67100	67500 ± 6750
Co	µg/L	<0.50	<0.50
Cu	µg/L	<10.0	<2.0
Fe	µg/L	<20.0	145 ± 14.5
Li	µg/L	187 ± 18.7	21.2 ± 2.1
Mg	µg/L	261000 ± 26100	20000 ± 2000
Mn	µg/L	1840 ± 184	172 ± 17.2
Mo	µg/L	<10.0	<2.0
P	µg/L	<500	<100
K	µg/L	22100 ± 2210	7300 ± 730
Ag	µg/L	<10.0	<2.0
Na	µg/L	2120000 ± 212000	436000 ± 43600
Tl	µg/L	<5.00	<1.00
Sn	µg/L	<10.0	<2.0
Ti	µg/L	<10.0	<2.0
U	µg/L	11.3 ± 1.13	1.69 ± 0.17
V	µg/L	<1.0	1.0 ± 0.1
Zn	µg/L	<20.0	50.2 ± 5.0
Cd	µg/L	<0.200	<0.040
Cr	µg/L	<2.00	<0.400
Ni	µg/L	<2.00	<2.00
Pb	µg/L	<0.500	<0.500
Sb	µg/L	<0.500	0.214 ± 0.041
As	µg/L	<2.00	<1.00
Se	µg/L	<2.00	<1.00

## 5. Summary

This is the first research report of the MICWEST project, included in the SAFER2028 programme. The objective of MICWEST is to study the performance of steel welds in low- and intermediate level waste (LILW) repository mimicking conditions. This will be done through defining the type of corrosion in welds and heat-affected zones (HAZ) in different conditions mimicking the different evolutionary stages of the repository, studying microbe-weldment interactions on steel surfaces and defining the role of different weldment types, material combinations in welds and post-weld cleaning methods on weld durability and corrosion resistance. The current report illuminates the background knowledge of the conditions assumed



to prevail in the repositories, and describes the selection of certain water types, materials and welding methods to be assessed within the project.

It is assumed that the repository will undergo evolution in its conditions and thus the conditions will change over time. This research will consider cases in which water will get into contact with the steel material and welds. In the first stages of the repository, porewater from the concrete present in the repository is going to have a major effect on the constituents of the water. Due to the ingress of the groundwater, the porewater will get mixed with the groundwater, and its influence will lessen until the water can be considered to be fully groundwater. In this report, thermodynamical simulations on the water chemistry are presented in order to improve the understanding of the principles of the interaction of groundwater with cured cement that contains concrete porewater. Moreover, baseline electrochemical assessment for the selected stainless steels is included for simulated porewater and groundwater at different pH.

Native groundwaters were collected and analysed, and recipes for simulants were formulated. The activity of the intrinsic groundwater microbes will be assessed for the next phase of the project, consisting of exposure tests.

The materials and the welding methods were selected to represent the components present in the repository:

- (1) Carbon steel containers to include the cut-up waste: carbon steel welded by submerged arc welding due to its high productivity and quality in workshop conditions, and MAG welding for its versatility in all-position butt and fillet welds in workshop and field on-site fabrication.
- (2) Weld between the reactor pressure vessel nozzle and plug to shut the reactor pressure vessel: the inside of the reactor pressure vessel clad with 321 stainless steel is welded with the plug material of stainless steel 316L with MAG welding, due to its versatility in all-position welds also in on-site fabrication.
- (3) Weld between the outside of the reactor pressure vessel nozzle and plug, and reactor pressure vessel and new lid: reactor pressure vessel steel is welded with stainless steel 316L (plug/lid) with MAG welding due to its versatility in all-position welds also in on-site fabrication.

These welds were manufactured to provide testing materials for the next phases, consisting of exposure tests. In addition, a part of the samples will be post-treated by either grinding or pickling.

## 6. References

---

- Ahlström, J. (2015) Corrosion of steel in concrete at various moisture and chloride levels, Master's thesis, Rapport 2015:133, Energiforsk AB, Stockholm, Sweden
- Äikäs, T., and Anttila, P. (2008), Repositories for low- and intermediate-level radioactive wastes in Finland, in Rempe, N.T., ed., Deep Geologic Repositories: Geological Society of America Reviews in Engineering Geology, v. XIX, p. 67–71, [https://doi.org/10.1130/2008.4119\(07\)](https://doi.org/10.1130/2008.4119(07))
- Anzai, Nakano, K., Nishio, K., & Matsukawa, K. (2006) Biofilm adhesion and microbially influenced corrosion of SUS304 welds exposed to dam water. *Welding International*, 20(9), 698–706. <https://doi.org/10.1533/wint.2006.3634>
- Beech, I. B., and Sunner, J. (2004). Biocorrosion: towards understanding interactions between biofilms and metals. *Curr. Opin. Biotechnol.* 15, 181–6. <https://doi.org/10.1016/j.copbio.2004.05.001>
- Bell, Lamminmäki, T., Alneberg, J., Andersson, A. F., Qian, C., Xiong, W., Hettich, R. L., Fruttschi, M., & Bernier-Latmani, R. (2020) Active sulfur cycling in the terrestrial deep subsurface. *The ISME Journal*, 14(5), 1260–1272. <https://doi.org/10.1038/s41396-020-0602-x>
- Bomberg, Lamminmäki, T., & Itävaara, M. (2016). Microbial communities and their predicted metabolic characteristics in deep fracture groundwaters of the crystalline bedrock at Olkiluoto, Finland. *Biogeosciences*, 13(21), 6031–6047. <https://doi.org/10.5194/bg-13-6031-2016>

- Carpén, L. (2008) Corrosion of Stainless Steel in Fire Protection Systems. VTT Research report No VTT-R-01556-08. <https://publications.vtt.fi/julkaisut/uuut/2008/PALOMIC Tutk rap final.pdf>
- Cernoušek, T., Ševců, A., Shrestha, R., Steinová, J., Kokinda, J., Vizelkova, K. (2020) Chapter 6: Microbially induced corrosion of container material in The Microbiology of Nuclear Waste Disposal. Elsevier, edited by Lloyd, Cherkouk, A., & Lloyd, J. R. San Diego: Elsevier, 2020.
- Dhaiveegan, P., Elangovan, N., Nishimura, T., & Rajendran, N. (2016). Corrosion behavior of 316L and 304 stainless steels exposed to industrial-marine-urban environment: field study. RSC Advances, 6(53), 47314–47324. <https://doi.org/10.1039/C6RA04015B>
- Fattah-alhosseini, A., Saatchi, A., Golozar, M. A., & Raeissi, K. (2009). The transpassive dissolution mechanism of 316L stainless steel. *Electrochimica Acta*, 54(13), 3645–3650. <https://doi.org/10.1016/j.electacta.2009.01.040>
- Freire, L., Carmezim, M. J., Ferreira, M. G. S., & Montemor, M. F. (2010). The passive behaviour of AISI 316 in alkaline media and the effect of pH: A combined electrochemical and analytical study. *Electrochimica Acta*, 55(21), 6174–6181. <https://doi.org/10.1016/j.electacta.2009.10.026>
- Garcia, M., Procópio, L. (2020) Distinct Profiles in Microbial Diversity on Carbon Steel and Different Welds in Simulated Marine Microcosm. *Curr Microbiol* 77, 967–978 (2020). <https://doi.org/10.1007/s00284-020-01898-4>
- Glasser FP (2011) Application of inorganic cements to the conditioning and immobilisation of radioactive wastes. In: Ojovan MI (ed) Handbook of advanced radioactive waste conditioning technologies. Woodhead, Oxford, pp 67–135
- Grenthe, I., Stumm, W., Laaksoharju, M., Nilsson, A-C. & Wikberg, P. 1992. Redox potentials and redox reactions in deep groundwater systems. *Chemical Geology*, Vol. 98, pp. 131-150.
- Hallbeck, L., & Pedersen, K. (2008). Characterization of microbial processes in deep aquifers of the Fennoscandian Shield. *Applied Geochemistry*, 23(7), 1796-1819.
- Hatanpää, E. (2006), Groundwater Sampling from Borehole HH-KR1 at Hästholmen, Loviisa, in 2004, Working Report 2006-40, Posiva Oy, Olkiluoto, Finland
- Hatanpää, E. (2006). Groundwater Sampling from Borehole HH-KR1 at Hästholmen, Loviisa, in 2004.
- Haveman, S., Pedersen, K. & Ruotsalainen, P. 1998. Microbial investigations of Olkiluoto, Hästholmen, Kivetty and Romuvaara groundwaters. Helsinki, Finland: Posiva Oy, Report POSIVA 98-09.40 p.
- Hegler, F., Posth, N. R., Jiang, J., & Kappler, A. (2008). Physiology of phototrophic iron (II)-oxidizing bacteria: implications for modern and ancient environments. *FEMS Microbiology Ecology*, 66(2), 250-260.
- Huang, Y., Shao, H., Wieland, E., Kolditz, O., Kosakowski, G. (2021), Two-phase transport in a cemented waste package considering spatio-temporal evolution of chemical conditions, *npj Materials Degradation* (2021) 5:4
- IAEA. (1998). Interim Storage of Radioactive Waste Packages.
- IAEA. (2009). Classification of Radioactive Waste.
- Jones, D. (1996). Principles and Prevention of Corrosion. Prentice Hall.
- Kari, O.-P. (2014) Long-term ageing of concrete structures in Finnish rock caverns as application facilities for low- and intermediate-level nuclear waste, Doctoral dissertations 9/2015, Aalto University, Espoo, Finland
- Kyröläinen, A., Lukkari, J. (1999) Ruostumattomat teräkset ja niiden hitsaus, Metalliteollisuuden kustannus, Helsinki, Finland.
- Li, Y. et al. (2018) Anaerobic microbiologically influenced corrosion mechanisms interpreted using bioenergetics and bioelectrochemistry: A review. *Journal of materials science & technology*. [Online] 34 (10), 1713–1718
- Liduíno, V.S., Cravo-Laureau, C., Noel, C., Carbon, A., Duran, R., Lutterbach, M. T., & Camporese Sérvulo, E. F. (2019) Comparison of flow regimes on biocorrosion of steel pipe weldments: Community composition and diversity of biofilms. *International Biodeterioration & Biodegradation*, 143, 104717–. <https://doi.org/10.1016/j.ibiod.2019.104717>
- Linhardt, P. (2010) Twenty years of experience with corrosion failures caused by manganese oxidizing microorganisms. *Materials and corrosion*. [Online] 61 (12), 1034–1039.
- Little, B., Wagner, P., and Mansfeld, F. (1992). An overview of microbiologically influenced corrosion. *Electrochim. Acta* 37, 2185–2194. [https://doi.org/10.1016/0013-4686\(92\)85110-7](https://doi.org/10.1016/0013-4686(92)85110-7)

- Lothenbach, B., Le Saout, G., Gallucci, E., Scrivener, K. (2008) Influence of limestone on the hydration of Portland cements, *Cement and Concrete Research* 38, 48-860
- Luukkonen, A., Pitkänen, P., Ruotsalainen, P., Leino-Forsman, H., & Snellman, M. (1999). Hydrogeochemical conditions at the Hästholmen site (No. POSIVA--99-26). Posiva Oy.
- Nordstrom, D.K., Ball, J.W., Donahoe, R.J. & Barton, C.C. 1989b. Fluid inclusions in the Stripa granite and their possible influence on the groundwater chemistry. *Geochimica et Cosmochimica Acta*, Vol. 53, pp. 1741-1755
- Nummi, O. (2018) Safety case for Loviisa LILW repository 2018 – Main report, LO1-T3552-00023, Fortum Power and Heat Oy, Loviisa, Finland
- Nummi, O. (2022) Fortum Oyj, personal communication, 09/2022
- Nuppenen-Puputti, M., Kietäväinen, R., Purkamo, L., Rajala, P., Itävaara, M., Kukkonen, I., & Bomberg, M. (2020) Rock Surface Fungi in Deep Continental Biosphere-Exploration of Microbial Community Formation with Subsurface In Situ Biofilm Trap. *Microorganisms (Basel)*, 9(1), 64–. <https://doi.org/10.3390/microorganisms9010064>
- Nuppenen-Puputti, M., Kietäväinen, R., Raulio, M., Soro, A., Purkamo, L., Kukkonen, I., & Bomberg, M. (2022) Epilithic Microbial Community Functionality in Deep Oligotrophic Continental Bedrock. *Frontiers in Microbiology*, 13, 826048–826048. <https://doi.org/10.3389/fmicb.2022.826048>
- Olsson, C.-O. A., & Landolt, D. (2003). Passive films on stainless steels—chemistry, structure and growth. *Electrochimica Acta*, 48(9), 1093–1104. [https://doi.org/10.1016/S0013-4686\(02\)00841-1](https://doi.org/10.1016/S0013-4686(02)00841-1)
- Pedersen. (1999) Subterranean microorganisms and radioactive waste disposal in Sweden. *Engineering Geology*, 52(3), 163–176. [https://doi.org/10.1016/S0013-7952\(99\)00004-6](https://doi.org/10.1016/S0013-7952(99)00004-6)
- Pedersen. (2013) Metabolic activity of subterranean microbial communities in deep granitic groundwater supplemented with methane and H<sub>2</sub>. *The ISME Journal*, 7(4), 839–. <https://doi.org/10.1038/ismej.2012.144>
- Pitkänen, P., Luukkonen, A., Ruotsalainen, P., Leino-Forsman, H. & Vuorinen, U. 1998. Geochemical modelling of groundwater evolution and residence time at the Kivetty site. Helsinki, Finland: Posiva Oy, Report POSIVA 98-07. 139 p.
- Pitkänen, P., Luukkonen, A., Ruotsalainen, P., Leino-Forsman, H., & Vuorinen, U. (1999). Geochemical modelling of groundwater evolution and residence time at the Olkiluoto site (No. POSIVA--98-10). Posiva Oy.
- Pitkänen, P., Luukkonen, A., Ruotsalainen, P., Leino-Forsman, H., & Vuorinen, U. (1999). Geochemical modelling of groundwater evolution and residence time at the Olkiluoto site.
- Pitkänen, P., Snellman, M. & Leino-Forsman, H. (1994) Geochemical modelling of the groundwater at the Olkiluoto site. Nuclear Waste Commission of Finnish Power Companies, Report YJT-94-10.
- Pitkänen, P., Snellman, M., Vuorinen, U. (1996) On the origin and chemical evolution of groundwater at the Olkiluoto site, POSVA-96-04, Posiva Oy, Helsinki, Finland.
- Pitkänen, P., Snellman, M., Vuorinen, U., & Leino-Forsman, H. (1996). Geochemical modelling study on the age and evolution of the groundwater at the Romuvaara site.
- Pitkäoja, J. (2019). Long-term safety assessment for disposal of VTT's decommissioning wastes in Loviisa LILW repository [Master's thesis]. University of Jyväskylä.
- Preece, C. M., Corrosion of steel in concrete. Stockholm 1982. KBS Teknisk rapport 82-19. 34p.
- Purkamo, Bomberg, M., Kietäväinen, R., Salavirta, H., Nyssönen, M., Nuppenen-Puputti, M., Ahonen, L., Kukkonen, I., & Itävaara, M. (2016) Microbial co-occurrence patterns in deep Precambrian bedrock fracture fluids. *Biogeosciences*, 13(10), 3091–3108. <https://doi.org/10.5194/bg-13-3091-2016>
- STUK 2018. Guide YVL D.5 Disposal of nuclear waste. Radiation and Nuclear Safety Authority
- Rajala, P. (2017). Microbially-induced corrosion of carbon steel in a geological repository environment: Dissertation. [Dissertation, University of Helsinki]. VTT Technical Research Centre of Finland. <https://publications.vtt.fi/pdf/science/2017/S155.pdf>
- Rajala, P., Bomberg, M., Vepsäläinen, M., Carpén, L. (2017) Microbial fouling and corrosion of carbon steel in alkaline deep groundwater, *Biofouling*, 33(2): 195-209.
- Rajala, P., Carpén, L., Vepsäläinen, M., Raulio, M., Huttunen-Saarivirta, E., Bomberg, M. (2016) Influence of carbon sources and concrete on microbially induced corrosion of carbon steel in subterranean groundwater environment, *CORROSION*, 72(12): 1565-1579.

- Rajala, P., Nuppenen-Puputti, M., Wheat, C.G., Carpen, L. (2022) Fluctuation in deep groundwater chemistry and microbial community and their impact on corrosion of stainless-steels, *Science of The Total Environment*, Volume 824, 153965, ISSN 0048-9697, <https://doi.org/10.1016/j.scitotenv.2022.153965>..
- Sedriks, A.J. (1996), *Corrosion of Stainless Steels*, 2nd Edition, Wiley-Interscience, New York, USA.
- Small, J., Nykyri, M., Helin, M., Hovi, U., Sarlin, T., and Itävaara, M. (2008). Experimental and modelling investigations of the biogeochemistry of gas production from low and intermediate level radioactive waste. *Appl. Geochemistry* 23, 1383–1418. <https://doi.org/10.1016/j.apgeochem.2007.11.020>.
- Small, J.S. & Vikman, M. (2020). Chapter 9: Microbial impacts on gas production in LLW/LIW in *The Microbiology of Nuclear Waste Disposal*. Elsevier, edited by Lloyd, Cherkouk, A., & Lloyd, J. R. San Diego: Elsevier, 2020.
- Somervuori, M., Isotahdon, E., Nuppenen-Puputti, M., Bomberg, M., Carpén, L., Rajala, P. (2021) A Comparison of Different Natural Groundwaters from Repository Sites—Corrosivity, Chemistry and Microbial Community. *Corros. Mater. Degrad.* 2021, 2, 603–624. <https://doi.org/10.3390/cmd2040032>
- STUK, Loviisan voimalaitos, Archived from the original ([http://www.stuk.fi/ydinturvallisuus/ydinvoimalaitokset/loviisa/fi\\_FI/loviisa/\\_print/](http://www.stuk.fi/ydinturvallisuus/ydinvoimalaitokset/loviisa/fi_FI/loviisa/_print/)) on 29 March 2012, [https://web.archive.org/web/20120329104516/http://www.stuk.fi/ydinturvallisuus/ydinvoimalaitokset/loviisa/fi\\_FI/loviisa/\\_print/](https://web.archive.org/web/20120329104516/http://www.stuk.fi/ydinturvallisuus/ydinvoimalaitokset/loviisa/fi_FI/loviisa/_print/)
- STUK, “Joint Convention on the Safety of Spent Fuel Management and on the Safety of Radioactive Waste Management. 6th Finnish National Report as referred to in Article 32 of the Convention,” Helsinki, Finland, STUK-B 218, 2017.
- Tandré, O. (2020), Review: Radionuclide leaching in concrete containment barriers, Research Report VTT-R-00116-20, VTT Technical Research Centre of Finland Ltd, Espoo, Finland.
- Tommila, A. (2021) Decommissioning and Final Disposal of Loviisa VVER-440 Reactor Pressure Vessel and its Internals, Master's Thesis, Lappeenranta-Lahti University of Technology LUT, Lappeenranta, Finland
- Tuunanen, J., Viitanen, P. (2014) On-Site Disposal of Radioactive Waste as a Part of Finnish Radioactive Waste Management System, WM2014 Conference, March 2 - 6, 2014, Phoenix, Arizona, USA.
- Urios, L., Mailliet, A., Dauzères, A., Flachet, M., & Magot, M. (2014). Tournemire argillite/carbon steel evolution under bacterial influence after 10 years of in situ interaction. *Corrosion engineering, science and technology*, 49(6), 554-561.
- Videla, H. A., and Herrera, L. K. (2005). Microbiologically influenced corrosion: looking to the future. *Int. Microbiol.* 8, 169–180. doi:im2305026 [pii]
- Vieno, T., and Nordman, H., (1998), VLJ (Voimalaitosjäte) Repository Safety Analysis Report TVO-1: Teollisuuden Voima Oy, Finland, 98 p.
- Wang, Xie, G.-J., Tian, N., Dang, C.-C., Cai, C., Ding, J., Liu, B.-F., Xing, D.-F., Ren, N.-Q., & Wang, Q. (2022) Anaerobic microbial manganese oxidation and reduction: A critical review. *The Science of the Total Environment*, 822, 153513–153513. <https://doi.org/10.1016/j.scitotenv.2022.153513>
- Whitman, G. W., Russell, R. P., & Altieri, V. J. (1924). Effect of Hydrogen-Ion Concentration on the Submerged Corrosion of Steel. *Industrial & Engineering Chemistry*, 16(7), 665–670. <https://doi.org/10.1021/ie50175a002>
- Winston Revie, R., and Uhlig, H. H. (2008) *Corrosion and Corrosion Control: An introduction to corrosion science and engineering*. 4th Edition. WILEY-VCH Verlag GmbH <https://doi.org/10.1179/000705972798323134>.
- Yasuyuki MI, Michiyoshi YA, Kazuya WA, Yasushi KI. (2002) Case Study on Microbiologically Influenced Corrosion of SUS316L welds (Materials, Metallurgy & Weldability). *Transactions of JWRI.* ;31(2):213-7.
- Ydinenergialaki (990/1987). (1987).
- Yim, M.-S. (2022). *Nuclear Waste Management* (Vol. 83). Springer Netherlands. <https://doi.org/10.1007/978-94-024-2106-4>
- Zhang, Y., Urquidi-Macdonald, M., Engelhardt, G. R., & Macdonald, D. D. (2012). Development of localized corrosion damage on low pressure turbine disks and blades: II. Passivity breakdown. *Electrochimica Acta*, 69, 12–18. <https://doi.org/10.1016/j.electacta.2012.01.023>



## 7. Appendix

---

### 7.1 List of abbreviations

CPW – concrete pore water  
DAPI – 4’6-diamidino-2-phenylindole  
DOC – dissolved organic carbon  
FPH – Fortum Power and Heat  
GMAW – gas-metal-arc welding  
GW – groundwater  
ILW – intermediate level waste  
LLW – low level waste  
MAG – metal active gas  
MAGs – metagenome-assembled genomes  
MIC – microbiologically influenced corrosion  
MIG – metal inert gas  
NPP – nuclear power plant  
OCP – open circuit potential  
PDP – potentiodynamic polarization  
PES – polyethersulfone  
PVS – pressure vessel steel  
RPV – reactor pressure vessel  
SAW – submerged-arc welding  
SHE – standard hydrogen electrode  
SRB – sulphate-reducing bacteria  
SS – stainless steel  
STUK – Säteilyturvakeskus, Radiation and Nuclear Safety Authority (STUK)  
TDS – with total dissolved solids  
TOC – total organic carbon  
TVO – Teollisuuden Voima  
VLLW – very low-level waste

### 7.2 OES results for Fe 37B steel by Eurofins

### 7.3 Water analysis report for the Loviisa groundwater by ALS Finland

### 7.4 Water analysis report for the Olkiluoto groundwater by ALS Finland

## Test report

<b>Requested by</b>	<b>VTT Technical Research Centre of Finland Ltd.</b> Vilma Ratia-Hanby, <a href="mailto:vilma.ratia-hanby@vtt.fi">vilma.ratia-hanby@vtt.fi</a> Kemistintie 3 FI-02150 Espoo, Finland
<b>Order ref.</b>	VTT order 775922, Jukka Maunumäki 19.4.2023
<b>Contact person</b>	<b>Eurofins Expert Services Oy</b> Eeki Airola Kivimiehentie 4, 02150 Espoo <a href="mailto:eekeirola@eurofins.fi">eekeirola@eurofins.fi</a>
<b>Sample details</b>	<b>One steel sample coded "MICWEST"</b>
<b>Methods</b>	The sample was analysed on the 26 <sup>th</sup> of April 2023 using an optical emission spectrometer ARL iSpark 8860 and the internal method "Analysis of metal samples with an ARL8860 OES device".
<b>Results</b>	The results are listed in Table 1. Measurement uncertainties are reported upon request.

**Table 1.** The test results.

Element	Result, %	Accredited	Determination limit, %
Carbon, C	<b>0.10</b>	Yes	0.01
Silicon, Si	<b>0.013</b>	Yes	0.005
Manganese, Mn	<b>0.57</b>	Yes	0.01
Sulphur, S	<b>0.008</b>	Yes	0.003
Phosphorus, P	<b>0.006</b>	Yes	0.006
Chromium, Cr	<b>0.01</b>	Yes	0.01
Nickel, Ni	<b>0.04</b>	Yes	0.01
Molybdenum, Mo	<b>&lt;0.01</b>	Yes	0.01
Copper, Cu	<b>0.02</b>	Yes	0.01
Aluminium, Al	<b>0.02</b>	Yes	0.02
Wolfram, W	<b>&lt;0.03</b>	No	0.03
Vanadium, V	<b>&lt;0.006</b>	Yes	0.006
Titan, Ti	<b>&lt;0.002</b>	No	0.002
Cobalt, Co	<b>0.014</b>	No	0.008
Boron, B	<b>&lt;0.0008</b>	No	0.0008
Niobium, Nb	<b>0.014</b>	Yes	0.004
Tin, Sn	<b>&lt;0.001</b>	No	0.001
Lead, Pb	<b>&lt;0.01</b>	No	-
Arsenic, As	<b>&lt;0.005</b>	No	0.005
Iron, Fe	(base)	No	-

**Espoo, 28.4.2023**

*Eeki Airola*

*Eeki Airola*

*Expert*

*Jouni Penttilä*

*Jouni Penttilä*

*Senior technician*

Distribution

Customer, electronically approved



## ANALYYSIRAPORTTI

Tilausnumero	: HL2302169	Tarjousnumero	: —
Asiakas	: Teknologian tutkimuskeskus VTT Oy	Projekti	: MICWEST
Yhteyshenkilö	: Maija Nuppenen-Puputti	Ostotilausnumero	: 778834
Osoite	: PL 1000 02044 VTT Suomi	Näytteenottaja	: Taru Lehtikuusi
Sähköposti	: maija.nuppenen-puputti@vtt.fi	Näytteenottokohde	: —
Puhelin	: —	Vastaanotetut näytteet	: 1
Sivu	: 1 / 5	Analysoidut näytteet	: 1
		Vastaanottopvm	: 2023-05-31 10:41
		Analyyseiden aloituspvm	: 2023-06-01
		Päiväys	: 2023-06-06 15:41

### Yleiset kommentit

Jos näytteenottoaikaa ei ole toimitettu, käytetään näytteenottoajan oletusarvoa 00:00 näytteenottopäivänä. Jos näytteenottopäivää ei ole toimitettu, käytetään oletusnäytteenottopäivää ja se näytetään sulkeissa ilman kellonaikaa.

Tämä raportti edustaa alkuperäistä analyysiraporttia. Raporttia ei saa muokata ja sen saa kopioida vain kokonaisuudessaan. Muusta kopioinnista on saatava erillinen kirjallinen lupa laboratorioilta. Analyysitulokset pätevät ainoastaan analysoiduille näytteille. Lisätietoa laboratorion vastuuvollisuuksista löytyy kotisivuiltamme <http://www.alsglobal.fi>

### Tilauksen kommentit

Näyte HL2302169/001, menetelmä W-METMSFL, W-NO3-SPC - määrittämissä on jouduttu nostamaan matriisihäiriöistä johtuen.

Allekirjoitukset	Asema
Jari Hautala	Maajohtaja

Laboratorio	: ALS Finland Oy	Nettisivu	: <a href="http://www.alsglobal.fi">www.alsglobal.fi</a>
Osoite	: Ruosilankuja 3 A 00390 Helsinki Suomi	Sähköposti	: <a href="mailto:asiakaspalvelu.hki@alsglobal.com">asiakaspalvelu.hki@alsglobal.com</a>
		Puhelin	: +358 10 470 1200

Sivu : 2 / 5  
 Tilausnumero : HL2302169  
 Asiakas : Teknologian tutkimuskeskus VTT Oy



## Analyysitulokset

Näyttematriisi: POHJAVESI

Asiakkaan näytetunnus  
 Laboratorion näytetunnus  
 Asiakkaan näytteenottopäivä/aika

LO5\_20230529

HL2302169-001

2023-05-29 00:00

Parametri	Tulos	MU	Yksikkö	LOR	Menetelmä	Laboratorio
<b>Fysikaaliset parametrit</b>						
W-PH-PCT/PR						
pH-arvo	7.73	± 0.08	-	1.00	W-PH-PCT	PR
<b>Yhdistelmäparametrit</b>						
W-DOC-IR/PR						
DOC	0.96	± 0.19	mg/L	0.50	W-DOC-IR	PR
W-TOC-IR/PR						
orgaanisen hiilen kokonaismäärä (TOC)	1.95	± 0.39	mg/L	0.50	W-TOC-IR	PR
<b>Epäorgaaniset parametrit</b>						
W-ALK-PCT/PR						
alkaliniteetti pH 4.5	1.76	± 0.211	mmol/L	0.150	W-ALK-PCT	PR
alkaliniteetti pH 8.3	<0.150	---	mmol/L	0.150	W-ALK-PCT	PR
W-CL-IC/PR						
kloridi	4980	± 746	mg/L	1.00	W-CL-IC	PR
W-CO2-FORMS/PR						
karbonaatit (CO3 2-)	0.0	± 0	mg/L	0.0	W-CO2F-CC2	PR
asiditeetti pH 8,3	0.157	± 0.024	mmol/L	0.150	W-ACID-PCT	PR
vetykarbonaatit (HCO3-)	107	± 12.9	mg/L	0.0	W-CO2F-CC2	PR
hiilidioksidi, kokonais	84.4	± 10.1	mg/L	0.0	W-CO2F-CC2	PR
asiditeetti pH 4.5	<0.150	---	mmol/L	0.150	W-ACID-PCT	PR
hiilidioksidi, vapaa	6.91	± 0.83	mg/L	0.0	W-CO2F-CC2	PR
aggressiivinen hiilidioksidi	4.80	± 0.58	mg/L	0.0	W-CO2F-CC2	PR
W-H2S-PHO/PR						
sulfidi (H2S)	<0.050	---	mg/L	0.050	W-H2S-PHO	CS
sulfidi (S2-)	<0.050	---	mg/L	0.050	W-H2S-PHO	CS
W-NH4-SPCL/PR						
ammonium	0.794	± 0.119	mg/L	0.026	W-NH4-SPC	PR
ammoniumtyppi	0.617	± 0.092	mg/L	0.020	W-NH4-SPC	PR
W-NO2-SPC/PR						
nitriitit	<0.0050	---	mg/L	0.0050	W-NO2-SPC	PR
nitriittityppi	<0.0020	---	mg/L	0.0020	W-NO2-SPC	PR
W-NO3-SPC/PR						
nitraatit	<0.66	---	mg/L	0.27	W-NO3-SPC	PR
nitraattityppi	<0.150	---	mg/L	0.060	W-NO3-SPC	PR
W-PO4O-SPC/PR						
fosfaatti	<0.040	---	mg/L	0.040	W-PO4O-SPC	PR
fosfaattifosfori	<0.013	---	mg/L	0.013	W-PO4O-SPC	PR
W-SO4-ICL/PR						
sulfaatti	576	± 86.4	mg/L	0.060	W-ANI-ENV	PR
<b>Kokonaismetallit</b>						

Sivu : 3 / 5  
Tilausnumero : HL2302169  
Asiakas : Teknologian tutkimuskeskus VTT Oy



Parametri	Tulos	MU	Yksikkö	LOR	Menetelmä	Laboratorio
<b>Kokonaismetallit - jatkuu</b>						
W-METMSFX6/PR						
Si	4.83	± 0.5	mg/L	0.0100	W-METMSFX6	PR
S	190	± 19.0	mg/L	0.500	W-METMSFX6	PR
<b>Liukoiset metallit</b>						
W-FE2D-PHO/PR						
Fe2+	0.017	± 0.007	mg/L	0.010	W-FE2D-PHO	CS
W-METFL-1/PR						
Hg	<0.0050	---	µg/L	0.0050	W-HG-AFSFLL	PR
Al	<20.0	---	µg/L	5.0	W-METMSFL5	PR
Ba	31.5	± 3.15	µg/L	0.50	W-METMSFL5	PR
Be	<1.00	---	µg/L	0.20	W-METMSFL5	PR
B	339	± 34	µg/L	10	W-METMSFL5	PR
Ca	671000	± 67100	µg/L	50	W-METMSFL5	PR
Co	<0.50	---	µg/L	0.50	W-METMSFL5	PR
Cu	<10.0	---	µg/L	1.0	W-METMSFL5	PR
Fe	<20.0	---	µg/L	2.0	W-METMSFL5	PR
Li	187	± 18.7	µg/L	1.0	W-METMSFL5	PR
Mg	261000	± 26100	µg/L	3.0	W-METMSFL5	PR
Mn	1840	± 184	µg/L	0.50	W-METMSFL5	PR
Mo	<10.0	---	µg/L	1.0	W-METMSFL5	PR
P	<500	---	µg/L	50.0	W-METMSFL5	PR
K	22100	± 2210	µg/L	50	W-METMSFL5	PR
Ag	<10.0	---	µg/L	1.0	W-METMSFL5	PR
Na	2120000	± 212000	µg/L	30	W-METMSFL5	PR
Tl	<5.00	---	µg/L	0.50	W-METMSFL5	PR
Sn	<10.0	---	µg/L	1.0	W-METMSFL5	PR
Ti	<10.0	---	µg/L	1.0	W-METMSFL5	PR
U	11.3	± 1.13	µg/L	0.10	W-METMSFL5	PR
V	<1.0	---	µg/L	1.0	W-METMSFL5	PR
Zn	<20.0	---	µg/L	2.0	W-METMSFL5	PR
Cd	<0.200	---	µg/L	0.020	W-METMSFLL1	PR
Cr	<2.00	---	µg/L	0.200	W-METMSFLL1	PR
Ni	<2.00	---	µg/L	2.00	W-METMSFLL1	PR
Pb	<0.500	---	µg/L	0.500	W-METMSFLL1	PR
Sb	<0.500	---	µg/L	0.050	W-METMSFLL1	PR
As	<2.00	---	µg/L	1.00	W-METMSFLL1	PR
Se	<2.00	---	µg/L	1.00	W-METMSFLL1	PR

Analyysiraportin tulososa päättyy tähän

Sivu : 4 / 5  
 Tilausnumero : HL2302169  
 Asiakas : Teknologian tutkimuskeskus VTT Oy



## Lyhyt menetelmäkuvas

Analyysimenetelmät	Menetelmäkuvaukset
W-FE2D-PHO	CZ_SOP_D06_07_116 (CSN ISO 6332) Raudan (II) määrittäminen spektrofotometrillä.
W-H2S-PHO	CZ_SOP_D06_07_015.A (CSN 83 0520-16:1978, CSN 83 0530-31:1980, SM 4500-S2- D) Sulfaanin ja sulfidin summan määrittäminen spektrofotometrisesti ja vapaan sulfaanin määrittäminen laskennallisesti mitatuista arvoista.
W-ACID-PCT	CZ_SOP_D06_02_073 (CSN 75 73 72) Emäsneutralointikapasiteetin (asiditeetin) määrittäminen potentiometrisella titrauksella.
W-ALK-PCT	CZ_SOP_D06_02_072 (CSN EN ISO 9963-1, CSN EN ISO 9963-2, CSN 75 7373, SM2320) Hapon neutralointikapasiteetin (alkaliniteetin) määrittäminen potentiometrisellä titrauksella, ja karbonaattikovuuden ja CO <sub>2</sub> -muotojen määrittäminen laskennallisesti mitatuista arvoista, sisältäen myös kokonaismineralisaation laskennan.
W-ANI-ENV	CZ_SOP_D06_02_068 (CSN EN ISO 10304-1) Liukoisen fluoridin, kloridin, nitriitin, bromidin, nitraatin ja sulfaatin määrittäminen ioniestekromatografilla ja nitriittityypen, nitraattityypen ja sulfaattirikin määrittäminen laskennallisesti mitatuista arvoista, sisältäen myös kokonaismineralisaation laskennan.
W-CL-IC	CZ_SOP_D06_02_068 (CSN EN ISO 10304-1) Liukoisen fluoridin, kloridin, nitriitin, bromidin, nitraatin ja sulfaatin määrittäminen ionikromatografisesti. Nitriitti- ja nitraattityypen sekä sulfaattirikin määrittäminen laskennallisesti mitatuista arvoista, sisältäen myös kokonaismineralisaation laskennan.
W-CO2F-CC2	CZ_SOP_D06_02_072 (CSN EN ISO 9963-1, CSN 75 7373) Happoneutralointikapasiteetin (alkaliniteetin) määrittäminen potentiometrisella titrauksella ja karbonaattikovuuden ja CO <sub>2</sub> -muotojen määrittäminen laskennallisesti mitatuista arvoista, sisältäen myös kokonaismineralisaation laskennan.
W-DOC-IR	CZ_SOP_D06_02_056 (CSN EN 1484, SM 5310) Orgaanisen hiilen kokonaismäärän (TOC), liukenevan orgaanisen hiilen (DOC), epäorgaanisen hiilen kokonaismäärän (TIC) ja kokonaishiilen (TC) määrittäminen IR-detektioinnilla.
W-HG-AFSFLL	CZ_SOP_D06_02_096 (US EPA 245.7, CSN EN ISO 17852) Elohopean määrittäminen fluoresenssispektrometrillä. Näyte suodatettiin mikro-suodattimella (huokoskoko 0.45 µm) ja siihen lisättiin typpihappoa ennen analyysia.
W-METMSFL5	CZ_SOP_D06_02_002 (US EPA 200.8, CSN EN ISO 17294-2, US EPA 6020A, CSN 75 7358) Alkuaineiden määrittäminen ICP-MS -tekniikalla ja yhdisteiden pitoisuuksien määrittäminen stoikiometristen laskentojen avulla mitatuista arvoista, sisältäen myös kokonaismineralisaation ja Ca+Mg summan laskennan. Näyte suodatettiin mikro-suodattimella (huokoskoko 0.45 µm) ja siihen lisättiin typpihappoa ennen analyysia.
W-METMSFLL1	CZ_SOP_D06_02_002 (US EPA 200.8, CSN EN ISO 17294-2, US EPA 6020A, CSN 75 7358) Alkuaineiden määrittäminen ICP-MS -tekniikalla ja yhdisteiden pitoisuuksien määrittäminen stoikiometristen laskentojen avulla mitatuista arvoista, sisältäen myös kokonaismineralisaation ja Ca+Mg summan laskennan. Näyte suodatettiin mikro-suodattimella (huokoskoko 0.45 µm) ja siihen lisättiin typpihappoa ennen analyysia.
W-METMSFX6	CZ_SOP_D06_02_002 (US EPA 200.8, CSN EN ISO 17294-2, US EPA 6020A, CSN 75 7358) Alkuaineiden määrittäminen ICP-MS-tekniikalla ja yhdisteiden pitoisuuksien määrittäminen stoikiometristen laskentojen avulla mitatuista arvoista, sisältäen myös kokonaismineralisaation laskennan ja Ca+Mg summan laskennan. Näytteeseen lisättiin typpihappoa ennen analyysia.
W-NH4-SPC	CZ_SOP_D06_02_019 (CSN EN ISO 11732, CSN EN ISO 13395, SM 4500-NO <sub>2</sub> -, SM 4500-NO <sub>3</sub> -) Ammoniumin ja ammonium-ionien summan sekä nitriitin ja nitriitti- ja nitraatti-ionien summan määrittäminen diskreetillä spektrofotometrillä. Nitriitin, nitraatin, ammoniumin, epäorgaanisen ja orgaanisen kokonaistypen sekä vapaan ja dissosioituneiden ammonium-ionien määrittäminen laskennallisesti mitatuista arvoista, sisältäen myös kokonaismineralisaation laskennan.
W-NO2-SPC	CZ_SOP_D06_02_019 (CSN EN ISO 11732, CSN EN ISO 13395, SM 4500-NO <sub>2</sub> (-), SM 4500-NO <sub>3</sub> (-)) Nitriitin summan ja nitriitti- ja nitraattityypen summan määrittäminen diskreetillä spektrofotometrillä sekä nitriitin ja nitraatin määrittäminen laskennallisesti mitatuista arvoista.
W-NO3-SPC	CZ_SOP_D06_02_019 (CSN EN ISO 11732, CSN EN ISO 13395, SM 4500-NO <sub>2</sub> (-), SM 4500-NO <sub>3</sub> (-)) Nitriitin summan ja nitriitti- ja nitraattityypen summan määrittäminen diskreetillä spektrofotometrillä sekä nitriitin ja nitraatin määrittäminen laskennallisesti mitatuista arvoista.
W-PH-PCT	CZ_SOP_D06_02_105 (CSN ISO 10523, US EPA 150.1, SM 4500-H+ B) pH:n määrittäminen potentiometrisesti.
W-PO4O-SPC	CZ_SOP_D06_02_022 (CSN EN ISO 6878 SM 4500-P) Ortofosfaatin määrittäminen diskreetillä spektrofotometrillä ja ortofosfaattifosforin määrittäminen laskennallisesti mitatuista arvoista sisältäen myös kokonaismineralisaation laskennan.
W-TOC-IR	CZ_SOP_D06_02_056 (CSN EN 1484, SM 5310) Orgaanisen hiilen kokonaismäärän (TOC), liunneen orgaanisen hiilen (DOC), epäorgaanisen hiilen kokonaismäärän (TIC) ja kokonaishiilen määrittäminen IR-detektioinnilla.



Sivu : 5 / 5  
Tilausnumero : HL2302169  
Asiakas : Teknologian tutkimuskeskus VTT Oy

**Lyhenteet:** **LOR** = Raportointiraja (Limit Of Reporting) edustaa normaalia raportointirajaa kyseessä olevalle parametrille ja menetelmälle. Huomioithan, että raportointiraja voi nousta esim. liian pienen näytämäärän vuoksi tai jos näyte joudutaan laimentamaan matriisihäiriöiden vuoksi.

**MU** = Mittausepävarmuus

\* = Merkki tuloksen yhteydessä tarkoittaa akkreditoimatonta analyysia.

**Mittausepävarmuus:**

*Mittausepävarmuus on ilmoitettu laajennettuna mittausepävarmuutena (dokumentin "Guide to the Expression of Measurement", JCGM 100:2008 Corrected version 2010" määritelmän mukaan), jossa on käytetty kattavuuskerrointa 2, jolloin luotettavuustaso on noin 95%. Mittausepävarmuus raportoidaan vain havaituille yhdisteille, joiden pitoisuudet ovat yli raportointirajan.*

*Alihankkijoiden mittausepävarmuus on yleensä annettu laajennettuna mittausepävarmuutena, jossa on käytetty kattavuuskerrointa 2. Laboratoriolta saa lisätietoja pyydettyessä. Asbesti- ja haitta-ainelaboratorio AHA-LAB Oy:n osalta edellisestä poikkeavat tiedot mittausepävarmuudesta on esitetty kunkin analyysimenetelmän kuvauksessa.*

**Analysoiva laboratorio**

	Laboratorio
CS	Analysoinnista vastaa ALS Czech Republic, s.r.o., Bendlova 1687/7 Ceska Lipa Tšekki 470 01 Akkreditointielin: CAI Akkreditointinumero: 1163, CSN EN ISO/IEC 17025:2018
PR	Analysoinnista vastaa ALS Czech Republic, s.r.o., Na Harfe 336/9 Praha 9 - Vysocany Tšekki 190 00 Akkreditointielin: CAI Akkreditointinumero: 1163, CSN EN ISO/IEC 17025:2018



## ANALYYSIRAPORTTI

Tilausnumero	: HL2302552	Tarjousnumero	: OF230123
Asiakas	: Teknologian tutkimuskeskus VTT Oy	Projekti	: MICWEST
Yhteyshenkilö	: Maija Nuppenen-Puputti	Ostotilausnumero	: 779764
Osoite	: PL 1000 02044 VTT Suomi	Näytteenottaja	: Taru Lehtikuusi
Sähköposti	: maija.nuppenen-puputti@vtt.fi	Näytteenottokohde	: ---
Puhelin	: ---	Vastaanotetut näytteet	: 1
Sivu	: 1 / 5	Analysoidut näytteet	: 1
		Vastaanottopvm	: 2023-06-15 14:31
		Analyyseiden aloituspvm	: 2023-06-16
		Päiväys	: 2023-06-22 15:18

### Yleiset kommentit

Jos näytteenottoaikaa ei ole toimitettu, käytetään näytteenottoajan oletusarvoa 00:00 näytteenottopäivänä. Jos näytteenottopäivää ei ole toimitettu, käytetään oletusnäytteenottopäivää ja se näytetään sulkeissa ilman kellonaikaa.

Tämä raportti edustaa alkuperäistä analyysiraporttia. Raporttia ei saa muokata ja sen saa kopioida vain kokonaisuudessaan. Muusta kopioinnista on saatava erillinen kirjallinen lupa laboratoriolta. Analyysitulokset pätevät ainoastaan analysoiduille näytteille. Lisätietoa laboratorion vastuuvollisuuksista löytyy kotisivuiltamme <http://www.alsglobal.fi>

### Tilauksen kommentit

Näyte HL2302552/001, menetelmä W-METMSFX - määrittämissärajat on jouduttu nostamaan matriisihäiriöstä johtuen.

Allekirjoitukset	Asema
Jari Hautala	Maajohtaja

Laboratorio	: ALS Finland Oy	Nettisivu	: <a href="http://www.alsglobal.fi">www.alsglobal.fi</a>
Osoite	: Ruosilankuja 3 A 00390 Helsinki Suomi	Sähköposti	: <a href="mailto:asiakaspalvelu.hki@alsglobal.com">asiakaspalvelu.hki@alsglobal.com</a>
		Puhelin	: +358 10 470 1200

Sivu : 2 / 5  
 Tilausnumero : HL2302552  
 Asiakas : Teknologian tutkimuskeskus VTT Oy



## Analyysitulokset

Näytematriisi: POHJAVESI

Asiakkaan näytetunnus  
 Laboratorion näytetunnus  
 Asiakkaan näytteenottopäivä/aika

<b>KR9_20230613</b>
HL2302552-001
2023-06-13 00:00

Parametri	Tulos	MU	Yksikkö	LOR	Menetelmä	Laboratorio
<b>Fysikaaliset parametrit</b>						
W-PH-PCT/PR						
pH-arvo	8.38	± 0.08	-	1.00	W-PH-PCT	PR
<b>Yhdistelmäparametrit</b>						
W-DOC-IR/PR						
DOC	7.19	± 1.44	mg/L	0.50	W-DOC-IR	PR
W-TOC-IR/PR						
orgaanisen hiilen kokonaismäärä (TOC)	7.80	± 1.56	mg/L	0.50	W-TOC-IR	PR
<b>Epäorgaaniset parametrit</b>						
W-ALK-PCT/PR						
alkaliniteetti pH 4.5	5.26	± 0.632	mmol/L	0.150	W-ALK-PCT	PR
alkaliniteetti pH 8.3	<0.150	---	mmol/L	0.150	W-ALK-PCT	PR
W-CL-IC/PR						
kloridi	623	± 93.4	mg/L	1.00	W-CL-IC	PR
W-CO2-FORMS/PR						
karbonaatit (CO3 2-)	3.65	± 0.44	mg/L	0.0	W-CO2F-CC2	PR
asiditeetti pH 8,3	<0.150	---	mmol/L	0.150	W-ACID-PCT	PR
vetykarbonaatit (HCO3-)	314	± 37.7	mg/L	0.0	W-CO2F-CC2	PR
hiilidioksidi, kokonais	229	± 27.5	mg/L	0.0	W-CO2F-CC2	PR
asiditeetti pH 4.5	<0.150	---	mmol/L	0.150	W-ACID-PCT	PR
hiilidioksidi, vapaa	0.0	± 0	mg/L	0.0	W-CO2F-CC2	PR
aggressiivinen hiilidioksidi	0.0	± 0	mg/L	0.0	W-CO2F-CC2	PR
W-H2S-PHO/PR						
sulfidi (H2S)	<0.050	---	mg/L	0.050	W-H2S-PHO	CS
sulfidi (S2-)	<0.050	---	mg/L	0.050	W-H2S-PHO	CS
W-NH4-SPCL/PR						
ammonium	0.240	± 0.036	mg/L	0.026	W-NH4-SPC	PR
ammoniumtyppi	0.186	± 0.028	mg/L	0.020	W-NH4-SPC	PR
W-NO2-SPC/PR						
nitriitit	<0.0050	---	mg/L	0.0050	W-NO2-SPC	PR
nitriittityppi	<0.0020	---	mg/L	0.0020	W-NO2-SPC	PR
W-NO3-SPC/PR						
nitraatit	<0.27	---	mg/L	0.27	W-NO3-SPC	PR
nitraattityppi	<0.060	---	mg/L	0.060	W-NO3-SPC	PR
W-PO4O-SPC/PR						
fosfaatti	0.167	± 0.033	mg/L	0.040	W-PO4O-SPC	PR
fosfaattifosfori	0.054	± 0.011	mg/L	0.013	W-PO4O-SPC	PR
W-SO4-ICL/PR						
sulfaatti	157	± 23.6	mg/L	0.060	W-ANI-ENV	PR
<b>Kokonaismetallit</b>						

Sivu : 3 / 5  
Tilausnumero : HL2302552  
Asiakas : Teknologian tutkimuskeskus VTT Oy



Parametri	Tulos	MU	Yksikkö	LOR	Menetelmä	Laboratorio
<b>Kokonaismetallit - jatkuu</b>						
W-METMSFX6/PR						
Si	6.72	± 0.7	mg/L	0.0100	W-METMSFX6	PR
S	51.5	± 5.1	mg/L	0.500	W-METMSFX6	PR
<b>Liukoiset metallit</b>						
W-FE2D-PHO/PR						
Fe2+	0.055	± 0.009	mg/L	0.010	W-FE2D-PHO	CS
W-METFL-1/PR						
Hg	<0.0050	---	µg/L	0.0050	W-HG-AFSFLL	PR
Al	5.8	± 0.6	µg/L	5.0	W-METMSFL5	PR
Ba	19.1	± 1.91	µg/L	0.50	W-METMSFL5	PR
Be	<0.20	---	µg/L	0.20	W-METMSFL5	PR
B	445	± 44	µg/L	10	W-METMSFL5	PR
Ca	67500	± 6750	µg/L	50	W-METMSFL5	PR
Co	<0.50	---	µg/L	0.50	W-METMSFL5	PR
Cu	<2.0	---	µg/L	1.0	W-METMSFL5	PR
Fe	145	± 14.5	µg/L	2.0	W-METMSFL5	PR
Li	21.2	± 2.1	µg/L	1.0	W-METMSFL5	PR
Mg	20000	± 2000	µg/L	3.0	W-METMSFL5	PR
Mn	172	± 17.2	µg/L	0.50	W-METMSFL5	PR
Mo	<2.0	---	µg/L	1.0	W-METMSFL5	PR
P	<100	---	µg/L	50.0	W-METMSFL5	PR
K	7300	± 730	µg/L	50	W-METMSFL5	PR
Ag	<2.0	---	µg/L	1.0	W-METMSFL5	PR
Na	436000	± 43600	µg/L	30	W-METMSFL5	PR
Tl	<1.00	---	µg/L	0.50	W-METMSFL5	PR
Sn	<2.0	---	µg/L	1.0	W-METMSFL5	PR
Ti	<2.0	---	µg/L	1.0	W-METMSFL5	PR
U	1.69	± 0.17	µg/L	0.10	W-METMSFL5	PR
V	1.0	± 0.1	µg/L	1.0	W-METMSFL5	PR
Zn	50.2	± 5.0	µg/L	2.0	W-METMSFL5	PR
Cd	<0.040	---	µg/L	0.020	W-METMSFLL1	PR
Cr	<0.400	---	µg/L	0.200	W-METMSFLL1	PR
Ni	<2.00	---	µg/L	2.00	W-METMSFLL1	PR
Pb	<0.500	---	µg/L	0.500	W-METMSFLL1	PR
Sb	0.214	± 0.041	µg/L	0.050	W-METMSFLL1	PR
As	<1.00	---	µg/L	1.00	W-METMSFLL1	PR
Se	<1.00	---	µg/L	1.00	W-METMSFLL1	PR

Analyysiraportin tulososa päättyy tähän



Sivu : 4 / 5  
 Tilausnumero : HL2302552  
 Asiakas : Teknologian tutkimuskeskus VTT Oy

## Lyhyt menetelmäkuvas

Analyysimenetelmät	Menetelmäkuvaukset
W-FE2D-PHO	CZ_SOP_D06_07_116 (CSN ISO 6332) Raudan (II) määrittäminen spektrofotometrillä.
W-H2S-PHO	CZ_SOP_D06_07_015.A (CSN 83 0520-16:1978, CSN 83 0530-31:1980, SM 4500-S2- D) Sulfaanin ja sulfidin summan määrittäminen spektrofotometrisesti ja vapaan sulfaanin määrittäminen laskennallisesti mitatuista arvoista.
W-ACID-PCT	CZ_SOP_D06_02_073 (CSN 75 73 72) Emäsneutralointikapasiteetin (asiditeetin) määrittäminen potentiometrisella titrauksella.
W-ALK-PCT	CZ_SOP_D06_02_072 (CSN EN ISO 9963-1, CSN EN ISO 9963-2, CSN 75 7373, SM2320) Hapon neutralointikapasiteetin (alkaliniteetin) määrittäminen potentiometrisellä titrauksella, ja karbonaattikovuuden ja CO <sub>2</sub> -muotojen määrittäminen laskennallisesti mitatuista arvoista, sisältäen myös kokonaismineralisaation laskennan.
W-ANI-ENV	CZ_SOP_D06_02_068 (CSN EN ISO 10304-1) Liukoisen fluoridin, kloridin, nitriitin, bromidin, nitraatin ja sulfaatin määrittäminen ioninestekromatografilla ja nitriittityypen, nitraattityypen ja sulfaattirikin määrittäminen laskennallisesti mitatuista arvoista, sisältäen myös kokonaismineralisaation laskennan.
W-CL-IC	CZ_SOP_D06_02_068 (CSN EN ISO 10304-1) Liukoisen fluoridin, kloridin, nitriitin, bromidin, nitraatin ja sulfaatin määrittäminen ionikromatografisesti. Nitriitti- ja nitraattityypen sekä sulfaattirikin määrittäminen laskennallisesti mitatuista arvoista, sisältäen myös kokonaismineralisaation laskennan.
W-CO2F-CC2	CZ_SOP_D06_02_072 (CSN EN ISO 9963-1, CSN 75 7373) Happoneutralointikapasiteetin (alkaliniteetin) määrittäminen potentiometrisella titrauksella ja karbonaattikovuuden ja CO <sub>2</sub> -muotojen määrittäminen laskennallisesti mitatuista arvoista, sisältäen myös kokonaismineralisaation laskennan.
W-DOC-IR	CZ_SOP_D06_02_056 (CSN EN ISO 20236, SM 5310) Orgaanisen hiilen kokonaismäärän (TOC), liukenevan orgaanisen hiilen (DOC), epäorgaanisen hiilen kokonaismäärän (TIC) ja kokonaishiilen (TC) määrittäminen IR-detektioinnilla.
W-HG-AFSFLL	CZ_SOP_D06_02_096 (US EPA 245.7, CSN EN ISO 17852) Elohopean määrittäminen fluoresenssispektrometrillä. Näyte suodatettiin mikro-suodattimella (huokoskoko 0.45 µm) ja siihen lisättiin typpihappoa ennen analyysia.
W-METMSFL5	CZ_SOP_D06_02_002 (US EPA 200.8, CSN EN ISO 17294-2, US EPA 6020A, CSN 75 7358) Alkuaineiden määrittäminen ICP-MS -tekniikalla ja yhdisteiden pitoisuuksien määrittäminen stoikiometristen laskentojen avulla mitatuista arvoista, sisältäen myös kokonaismineralisaation ja Ca+Mg summan laskennan. Näyte suodatettiin mikro-suodattimella (huokoskoko 0.45 µm) ja siihen lisättiin typpihappoa ennen analyysia.
W-METMSFLL1	CZ_SOP_D06_02_002 (US EPA 200.8, CSN EN ISO 17294-2, US EPA 6020A, CSN 75 7358) Alkuaineiden määrittäminen ICP-MS -tekniikalla ja yhdisteiden pitoisuuksien määrittäminen stoikiometristen laskentojen avulla mitatuista arvoista, sisältäen myös kokonaismineralisaation ja Ca+Mg summan laskennan. Näyte suodatettiin mikro-suodattimella (huokoskoko 0.45 µm) ja siihen lisättiin typpihappoa ennen analyysia.
W-METMSFX6	CZ_SOP_D06_02_002 (US EPA Method 200.8, CSN EN ISO 17294-2, US EPA Method 6020A, CSN 75 7358) Alkuaineiden määrittäminen ICP-MS-tekniikalla ja yhdisteiden pitoisuuksien määrittäminen stoikiometristen laskentojen avulla mitatuista arvoista, sisältäen myös kokonaismineralisaation laskennan ja Ca+Mg summan laskennan. Näytteeseen lisättiin typpihappoa ennen analyysia.
W-NH4-SPC	CZ_SOP_D06_02_019 (CSN EN ISO 11732, CSN EN ISO 13395, SM 4500-NO <sub>2</sub> -, SM 4500-NO <sub>3</sub> -) Ammoniumin ja ammonium-ionien summan sekä nitriitin ja nitriitti- ja nitraatti-ionien summan määrittäminen diskreetillä spektrofotometrillä. Nitriitin, nitraatin, ammoniumin, epäorgaanisen ja orgaanisen kokonaistypen sekä vapaan ja dissosioituneiden ammonium-ionien määrittäminen laskennallisesti mitatuista arvoista, sisältäen myös kokonaismineralisaation laskennan.
W-NO2-SPC	CZ_SOP_D06_02_019 (CSN EN ISO 11732, CSN EN ISO 13395, SM 4500-NO <sub>2</sub> (-), SM 4500-NO <sub>3</sub> (-)) Nitriitin summan ja nitriitti- ja nitraattityypen summan määrittäminen diskreetillä spektrofotometrillä sekä nitriitin ja nitraatin määrittäminen laskennallisesti mitatuista arvoista.
W-NO3-SPC	CZ_SOP_D06_02_019 (CSN EN ISO 11732, CSN EN ISO 13395, SM 4500-NO <sub>2</sub> (-), SM 4500-NO <sub>3</sub> (-)) Nitriitin summan ja nitriitti- ja nitraattityypen summan määrittäminen diskreetillä spektrofotometrillä sekä nitriitin ja nitraatin määrittäminen laskennallisesti mitatuista arvoista.
W-PH-PCT	CZ_SOP_D06_02_105 (CSN ISO 10523, US EPA 150.1, SM 4500-H+ B) pH:n määrittäminen potentiometrisesti.
W-PO4O-SPC	CZ_SOP_D06_02_022 (CSN EN ISO 6878 SM 4500-P) Ortofosfaatin määrittäminen diskreetillä spektrofotometrillä ja ortofosfaattifosforin määrittäminen laskennallisesti mitatuista arvoista sisältäen myös kokonaismineralisaation laskennan.
W-TOC-IR	CZ_SOP_D06_02_056 (CSN EN ISO 20236, SM 5310) Orgaanisen hiilen kokonaismäärän (TOC), liukenevan orgaanisen hiilen (DOC), epäorgaanisen hiilen kokonaismäärän (TIC) ja kokonaishiilen määrittäminen IR-detektioinnilla.



Sivu : 5 / 5  
Tilausnumero : HL2302552  
Asiakas : Teknologian tutkimuskeskus VTT Oy

**Lyhenteet:** **LOR** = Raportointiraja (Limit Of Reporting) edustaa normaalia raportointirajaa kyseessä olevalle parametrille ja menetelmälle. Huomioithan, että raportointiraja voi nousta esim. liian pienen näytämäärän vuoksi tai jos näyte joudutaan laimentamaan matriisihäiriöiden vuoksi.

**MU** = Mittausepävarmuus

\* = Merkki tuloksen yhteydessä tarkoittaa akkreditoimatonta analyysia.

**Mittausepävarmuus:**

*Mittausepävarmuus on ilmoitettu laajennettuna mittausepävarmuutena (dokumentin "Guide to the Expression of Measurement", JCGM 100:2008 Corrected version 2010" määritelmän mukaan), jossa on käytetty kattavuuskerrointa 2, jolloin luotettavuustaso on noin 95%. Mittausepävarmuus raportoidaan vain havaituille yhdisteille, joiden pitoisuudet ovat yli raportointirajan.*

*Alihankkijoiden mittausepävarmuus on yleensä annettu laajennettuna mittausepävarmuutena, jossa on käytetty kattavuuskerrointa 2. Laboratoriolta saa lisätietoja pyydettyäessä. Asbesti- ja haitta-ainelaboratorio AHA-LAB Oy:n osalta edellisestä poikkeavat tiedot mittausepävarmuudesta on esitetty kunkin analyysimenetelmän kuvauksessa.*

**Analysoiva laboratorio**

	Laboratorio
CS	Analysoinnista vastaa ALS Czech Republic, s.r.o., Bendlova 1687/7 Ceska Lipa Tšekki 470 01 Akkreditointielin: CAI Akkreditointinumero: 1163, CSN EN ISO/IEC 17025:2018
PR	Analysoinnista vastaa ALS Czech Republic, s.r.o., Na Harfe 336/9 Praha 9 - Vysocany Tšekki 190 00 Akkreditointielin: CAI Akkreditointinumero: 1163, CSN EN ISO/IEC 17025:2018